Abrogation of glucosidase I–mediated glycoprotein deglucosylation results in a sick phenotype in fission yeasts: Model for the human MOGS-CDG disorder

Received for publication, July 12, 2018, and in revised form, October 30, 2018 Published, Papers in Press, November 2, 2018, DOI 10.1074/jbc.RA118.004844

Giovanna L. Gallo[‡1], Ayelén Valko[‡1,2], Sofía I. Aramburu[‡2], Emiliana Etchegaray[‡2], Christof Völker[§], Armando J. Parodi[‡3], and Cecilia D'Alessio[‡¶3,4]

From the [‡]Fundación Instituto Leloir–IIBBA, CONICET, Buenos Aires C1405BWE, Argentine, the [§]Institute of Biochemistry and Molecular Biology Medical Faculty, University of Bonn, 53115 Bonn, Germany, and the [¶]Departamento de Fisiología, Biología Molecular y Celular, Facultad de Ciencias Exactas y Naturales, Universidad de Buenos Aires, Buenos Aires C1428EGA, Argentine

Edited by Gerald W. Hart

Glucosidase I (GI) removes the outermost glucose from protein-linked $Glc_3Man_9GlcNAc_2$ (G3M9) in the endoplasmic reticulum (ER). Individuals with congenital disorders of glycosylation MOGS-CDG bear mutations in the GI-encoding gene (*gls1*). Although GI absence has been reported to produce lethality in *Schizosaccharomyces pombe* yeasts, here we obtained two viable Δ*gls1* mutants, one with a very sick but not lethal phenotype (Δ*gls1-S*) and the other with a healthier one (Δ*gls1-H*). The sick strain displayed only G3M9 as an ER protein–linked oligosaccharide, whereas the healthier strain had both G3M9 and $Man_9GlcNAc_2$. The lipid-linked oligosaccharide patterns of the two strains revealed that the most abundantly formed glycans were G3M9 in Δ*gls1-S* and $Glc_2Man_9GlcNAc_2$ in Δ*gls1-H*, suggesting reduced Alg10p glucosyltransferase activity in the Δ*gls1-H* strain. A mutation in the *alg10*$^+$ gene was indeed observed in this strain. Our results indicated that abrogated G3M9 deglucosylation was responsible for the severe defects observed in Δ*gls1-S* cells. Further studies disclosed that the defects could not be ascribed to disruption of glycoprotein entrance into calnexin-folding cycles, inhibition of the oligosaccharyltransferase by transfer reaction products, or reduced proteasomal degradation of misfolded glycoproteins. Lack of triglucosylated glycoprotein deglucosylation neither significantly prevented glycan elongation in the Golgi nor modified the overall cell wall monosaccharide composition. Nevertheless, it resulted in a distorted cell wall and in the absence of underlying ER membranes. Furthermore, Golgi expression of human endomannosidase partially restored normal growth in Δ*gls1-S* cells. We propose that accumulation of G3M9-bearing glycoproteins is toxic and at least partially responsible for defects observed in MOGS-CDG.

N-Glycans have multiple functions in the secretory pathway as they influence protein folding in the ER[5] and, after being remodeled in the Golgi, mediate interactions among cells and with the environment. It is not surprising then that genetic defects resulting in either their absence in normally occupied glycoprotein sites or in formation of aberrant *N*-glycan structures have a dramatic impact on many intra- and extracellular functions.

N-Glycosylation is one of the most frequent post-translational modifications of proteins following the secretory pathway. It starts with the initial *en bloc* transfer of glycan G3M9[6] (Fig. 1*A*) from a step-by-step prebuilt dolichol pyrophosphate derivative (Dol-PP) to Asn residues in the consensus sequence Asn-Xaa-Ser/Thr (Xaa≠Pro) in proteins entering the ER. The reaction is catalyzed by the oligosaccharyltransferase (OST), a multimeric membrane complex (Fig. 1*B*) (1–3). Addition of glycans facilitates *per se* protein folding as it provides bulky hydrophilic groups that help keeping folding intermediates in solution. *N*-Glycan processing by glycosidases and glucosyltransferases starts in the ER immediately after glycan transfer. Glycan remodeling plays a determining role in the mechanism of quality control of glycoprotein folding (4). Briefly, the glycan G3M9 transferred to Asn residues is first deglucosylated by GI, a type II membrane protein with a luminal hydrolytic domain that removes the outermost Glc of the glycan (residue *n*, Fig. 1*A*). The G2M9 thus produced is then deglucosylated by glucosidase II (GII) that successively generates G1M9 and M9 by removing the remaining glucose residues (*l* and *m*, Fig. 1*A*). G1M9 may be regenerated from M9 by the UDP-Glc:glycoprotein glucosyltransferase (UGGT), a protein conformation sensor that

This work was supported in part by the National Research Council (CONICET, Argentina) Grant PIP-11220150100759. The authors declare that they have no conflicts of interest with the contents of this article.
This article contains Figs. S1–S5 and Table S1.

[1] Both authors are CONICET fellows.
[2] These authors contributed equally to this work.
[3] Both authors are Career Investigators of the National Research Council (CONICET, Argentina).
[4] To whom correspondence should be addressed: Fundación Instituto Leloir, Av. Patricias Argentinas 435, Buenos Aires C1405BWE, Argentina. Tel.: 5411-5238-7500 (Ext. 2302); Fax: 5411-5238-7501; E-mail: cdalessio@leloir.org.ar.

[5] The abbreviations used are: ER, endoplasmic reticulum; CDG, congenital disorders of glycosylation; CNX, calnexin; Endo H, endo-β-*N*-acetylglucosaminidase H; GI, glucosidase I; GII, glucosidase II; LLO, lipid-linked oligosaccharide; NLO, protein-linked oligosaccharide; UGGT, UDP-Glc:glycoprotein glucosyltransferase; OST, oligosaccharyltransferase; ERAD, ER-associated degradation; ANOVA, analysis of variance; Dol-PP, dolichol pyrophosphate; NM-DNJ, *N*-methyl-deoxynojirimycin; TEM, transmission electron microscopy; hEM, human endomannosidase; fw, forward; HRP, horseradish peroxidase; CST, castanospermine.
[6] In glycan structures, Glc is abbreviated as G; Man is M; and GlcNAc is omitted. Thus, G3M9 is $Glc_3Man_9GlcNAc_2$; G2M9 is $Glc_2Man_9GlcNAc_2$; and M9 is $Man_9GlcNAc_2$, for example.

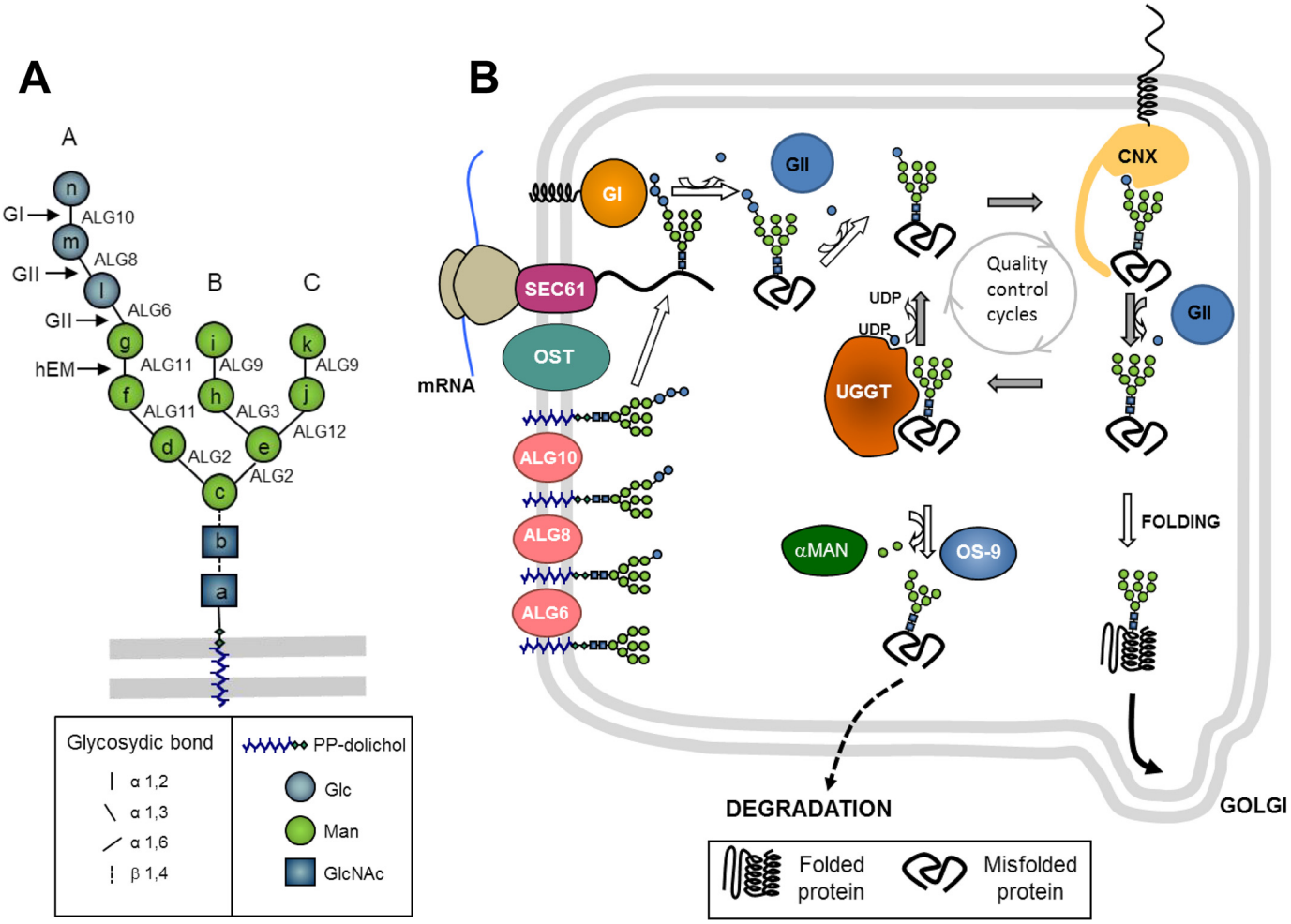

Figure 1. *N*-Glycosylation, *N*-glycan processing, and quality control of glycoprotein folding in the ER. *A,* synthesis and structure of glycan G3M9 transferred to proteins in *N*-glycosylation. The glycan is built in the ER membrane by the step by step addition of single monosaccharides to dolichol-P following the order of letters (*a, b, c, d* . . .) by the indicated *ALG* glycosyltransferases. It starts at the cytoplasmic side of the ER membrane, and once the structure Dol-PP-M5 is formed the glycan flips to the lumen of the ER where synthesis is completed. Arm A (residues *d, f, g,* and *l*–*n*), arm B (residues *h* and *l*), arm C (residues *j* and *k*) of the glycan, sites of GI and GII trimming in the ER *after* transference, and site of expressed Golgi human endomannosidase trimming are indicated. *B,* glycan transfer, *N*-glycan processing and ER quality control of glycoprotein folding. The last three steps of Dol-PP-G3M9 synthesis are shown. The OST complex transfers the glycan to the consensus sequence N*X*(S/T)(*X*≠P) of proteins entering into the ER through the Sec61 translocon. GI removes Glc *n* and GII removes Glc *m*. Monoglucosylated glycans interact with CNX, which facilitates glycoprotein folding. GII removes Glc *l* and folded glycoproteins exit the ER. Unfolded proteins are recognized by UGGT, which adds back Glc *l*. Glycoproteins that fail to properly fold after several reglucosylation–deglucosylation cycles are demannosylated by ER α-mannosidases (*αMAN*), recognized then by lectin OS9, and retrotranslocated to the cytosol for degradation in proteasomes (ERAD). Monosaccharide symbols follow the Symbol Nomenclature for Glycans (SNFG) system (49).

adds a Glc (residue *l*, Fig. 1*A*) exclusively to proteins that have not yet acquired their native conformation (5, 6). Monoglucosylated glycan-bearing glycoproteins produced either by de-glucosylation of the transferred glycan or by re-glucosylation by UGGT may interact with calnexin (CNX) and/or calreticulin, two ER-resident lectin chaperones that specifically recognize monoglucosylated structures. Glycoprotein–lectin interactions enhance folding efficiency and allow participation of a protein-disulfide protein isomerase (ERp57) in the folding process. In addition, they prevent Golgi exit of folding intermediates and irreparably misfolded glycoproteins (Fig. 1*B*). Cycles of glucosylation and deglucosylation catalyzed by the opposite activities of UGGT and GII continue until proper folding is achieved (Fig. 1*B*) (4). Folded glycoproteins pursue their transit through the secretory pathway where their glycans are further modified in the Golgi. Irreversibly misfolded glycoproteins are demannosylated and eventually retrotranslocated to the cytosol to be degraded in proteasomes in a process known as ER-associated degradation (ERAD).

The congenital disorders of glycosylation (CDG) are a group of more than 100 human inherited syndromes, most of them (70%) produced by deficiencies in protein *N*-glycosylation pathways (7). The clinical features of these disorders involve many organ systems but are especially common in the nervous, hepatic, visual, and immune systems. Patients display pathologies that include delayed growth, developmental disabilities, low muscle tone, visual problems, and incomplete brain development. Type I CDG are caused by defects in the biosynthesis of lipid-linked oligosaccharides (LLO) and their transfer to proteins, whereas type II CDG are caused by defects in the glycan processing of protein-linked oligosaccharides (NLO). The first type results in glycoprotein hypoglycosylation (normally occupied glycosylation sites are empty), but the remaining glycans

have almost normal structures, and in the second type there is a normal occupation of glycosylation sites, but the attached glycans have abnormal structures (7). Regarding the type II diseases, MOGS-CDG (also known as CDG-IIb) is produced by mutations in GI, the enzyme responsible for the first step in *N*-glycan processing (Fig. 1). The clinical course of the disease is progressive and characterized by multiple neurological complications, severe hypogammaglobulinemia, hepatomegaly, hypoventilation, feeding problems, seizures, and sometimes a fatal outcome (8, 9).

Contrary to the more commonly used yeast *Saccharomyces cerevisiae*, which lacks UGGT, the fission yeast *Schizosaccharomyces pombe* has conserved all components of the early *N*-glycosylation steps and the quality control of glycoprotein folding mechanism present in mammalian cells, and it has also been extensively used as a model organism to study those processes (4, 10). In an attempt to understand the role of GI in the molecular bases of MOGS-CDG, we obtained two haploid strains of the fission yeast *S. pombe* lacking the gene coding for GI (Δ*gls1*). Surprisingly, one of the strains showed a severe growth defect, and the other displayed an almost normal growth rate. We then analyzed NLO and LLO patterns produced by both strains. Our results suggest that a suppression of the mutant phenotype is caused by a simultaneous mutation in the *alg10*$^+$ gene in the strain that displayed a relieved growth rate. As the protein encoded by that gene is responsible for the addition of the outermost glucose to the Dol-PP derivative, we concluded that accumulation of three Glc moieties in the newly synthesized glycoproteins is the main cause of the growth defect in GI mutants. We propose that at least part of the defects observed in MOGS-CDG patients are caused by the accumulation of triglucosylated glycoproteins.

Results

Knockout of GI-encoding gene produces severe morphological and growth defects in the fission yeast S. pombe

According to an analysis of a genome-wide set of gene deletions in the fission yeast *S. pombe*, deletion of the GI-encoding gene (Δ*gls1* mutants) is apparently lethal (11). This is in contrast to what was reported for *S. cerevisiae*, in which mutants lacking the GI-encoding gene are viable (12) but in agreement with the report of patients in which mutations in GI-encoding gene result in MOGS-CDG with severe and sometimes lethal pathologies (8, 13). In an attempt to understand the role of GI in MOGS-CDG, we induced meiosis and sporulation in a heterozygous Δ*gls1*/+ diploid *S. pombe* strain. We were able to obtain two viable Δ*gls1* haploid strains that arose from spores of the same tetrad (Fig. 2*A*). One of the strains (Δ*gls1-S*) showed a very sick but not lethal growth defect. Surprisingly, the other strain (Δ*gls1-H*), although genetically also a Δ*gls1* knockout mutant, displayed a much healthier phenotype (Fig. 2*B*). We compared the growth-rate parameters in rich liquid medium of both Δ*gls1* mutants with that of *WT* and recorded that although the sick Δ*gls1-S* strain had all the growing parameters altered, *i.e.* an 8 times longer lag phase (32 h *versus* 4 h, $p = 0.005$), a 4-fold increase in the duplication time at the middle of the exponential phase ($p = 0.027$), and half the maximal $A_{600\ nm}$ at the stationary phase ($p = 0.045$), the same growth parameters of the healthier Δ*gls1-H* strain were significantly improved, with a shorter lag time (8 h), a duplication time twice as fast than that of Δ*gls1-S* strain ($p = 0.045$), and only a moderate reduction in the cell density at the stationary phase (Table S1).

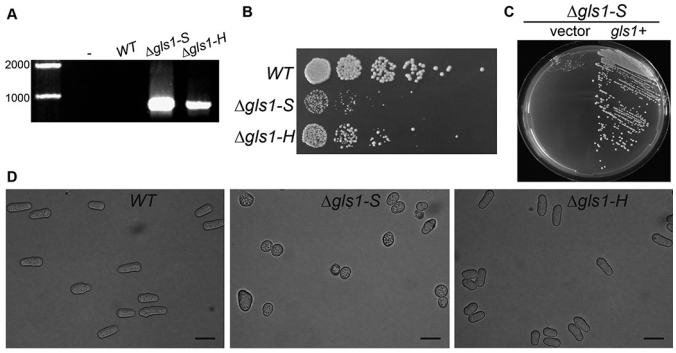

Figure 2. Lack of GI-encoding gene (*gls1*$^+$) produces severe growth and morphological defects in *S. pombe*. *A,* genomic characterization of *S. pombe* Δ*gls1*-S and Δ*gls1*-H strains. PCRs were performed using primers that hybridize inside and outside the knockout insertion cassette (NatMX fw and gls1–3′NC, respectively) and the indicated boiled yeast sister colonies as DNA template. *B,* growth of *S. pombe WT*, Δ*gls1*-S, and Δ*gls1*-H in solid media. *WT* and mutant cells were grown up to $A_{600\ nm} = 1$, and drops (5 μl) of 10-fold dilutions were plated on YES. Plates were incubated 72 h at 28 °C. *C,* reversion of the sick phenotype of Δ*gls1*-S cells by complementation with *gls1*$^+$ gene. Competent Δ*gls1*-S cells were transformed either with vector alone or with vector carrying *gls1*$^+$ gene. Leu$^+$ arising transformants were streaked in MM supplemented with adenine and uracil and grown for 72 h. *D,* morphology of Δ*gls1*-S and Δ*gls1*-H mutants. Yeast cultures at $A_{600\ nm} = 1$ were observed under a transmission microscope with a ×100 objective. *Bar,* 10 μm.

Complementation of the sick Δ*gls1-S* mutant with gene *gls1*$^+$ restored a normal growth phenotype, indicating that the absence of such gene was responsible for the observed defect in the mutant (Fig. 2*C*). The Δ*gls1-S* mutants cells observed under the microscope showed an aberrant morphology, with a reduced size and a rounded shape that tended to clump when compared with both *WT* and the healthier Δ*gls1-H* cells, suggesting that some kind of suppression had occurred in the last strain (Fig. 2*D*) (14).

NLO and LLO produced by Δgls1 mutants

To understand the phenotypic differences between both Δ*gls1* sick and healthier mutants, we first inspected the differences in the NLOs produced *in vivo* in the ER by *WT*, Δ*gls1-S,* and Δ*gls1-H* strains. Cells were labeled for 15 min with [^{14}C]Glc in the absence of any glucosidase inhibitor and in the presence of 5 mM DTT to preclude glycoprotein ER exit. *WT* cells rapidly trimmed protein-linked glycans from the transferred G3M9 structure to M9 by the sequential action of GI and GII (Fig. 3*A* and see Fig. 1). The severely affected Δ*gls1-S* cells showed the *N*-glycan pattern expected for a Δ*gls1* mutant, as these mutant cells are unable to hydrolyze the transferred G3M9 glycans and thus accumulate such structures (Fig. 3*B*). However, the healthier Δ*gls1-H* cell glycan pattern showed a further *N*-glycan processing to M9 (Fig. 3*C*), which was delayed when GI and GII were partially inhibited upon addition of castanospermine (CST) and *N*-methyl-deoxynojirimycin (NM-DNJ) (Fig. 3*D*).

Δ*gls1-H* strain showed a significant amount of glucose-free NLOs containing nine Man units similar to those produced by

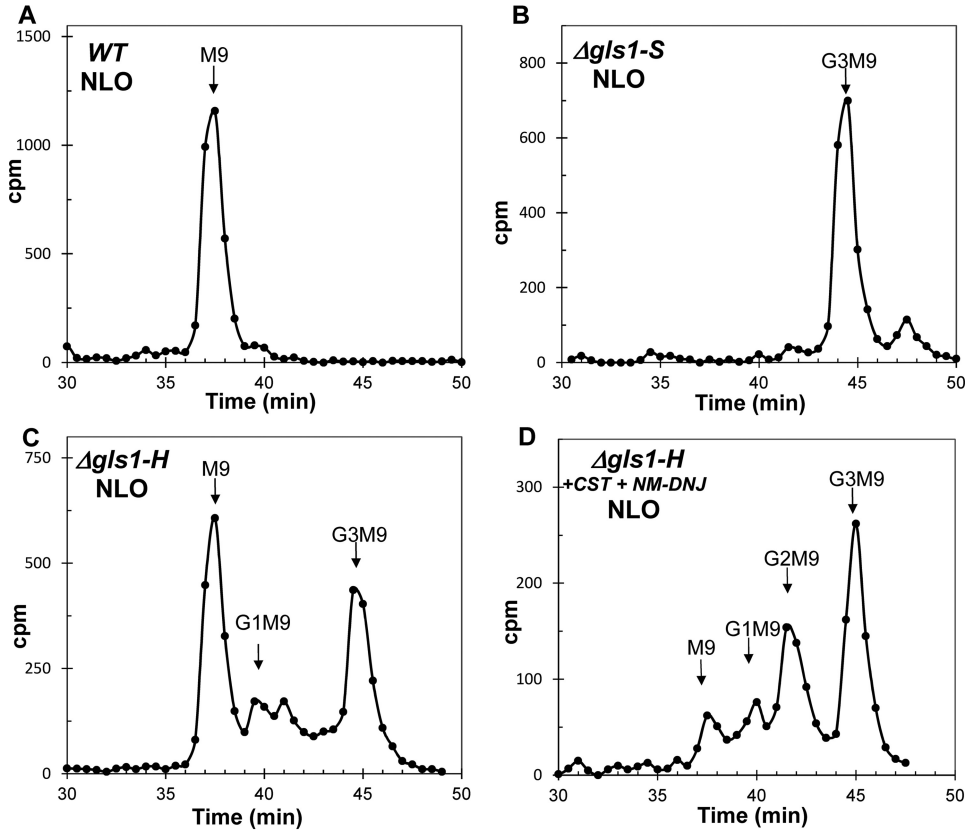

Figure 3. NLOs were synthesized *in vivo* by *S. pombe* mutants *WT* (*A*), Δ*gls1-S* (*B*), and Δ*gls1-H* (*C*). *S. pombe* exponentially growing cultures were washed and labeled with 5 mM [^{14}C]Glc for 15 min in the presence of 5 mM DTT and 3.5 mM kifunensine (an ER α-mannosidase inhibitor). *D,* Δ*gls1-H* cells were additionally labeled in the presence of the glucosidase inhibitors CST and NM-DNJ. Endo H–sensitive *N*-glycans were purified, run on paper chromatography in 1-propanol/nitromethane/water (5:2:4), eluted, and further resolved by HPLC. Positions of standards are indicated by *arrows*.

WT cells. This result cannot be explained by either a partial activity of GI, as the knockout strain has a large coding-sequence deleted, or by the presence of another GI-like activity in the ER (15). We hypothesized that the unexpected *N*-glycan pattern observed in Δ*gls1-H* strain could be explained by an incomplete LLO synthesis. Thus, we analyzed the LLO pattern synthesized *in vivo* by *WT* and Δ*gls1-H* mutant cells. As expected, almost all *WT* LLOs had a G3M9 structure (Fig. 4*A*). However, in Δ*gls1-H* mutant cells G2M9 was the main LLO present (Fig. 4*B*). The pattern resembled that produced by mutants in the gene coding the glucosyltransferase that adds the outermost Glc to the glycan in Dol-PP–G3M9 biosynthesis (Δ*alg10* mutants, Fig. 1) (16). Thus, the NLO pattern produced by Δ*gls1-H* mutants in which a large amount of M9 glycans was produced is most probably due to a partial defect in the biosynthesis of the LLO that is processed to G1M9 and M9 by GII upon transfer to proteins. The remaining G3M9 in glycoproteins of Δ*gls1-H* mutants could be explained by the small amount of G3M9 LLO in this strain that is transferred to proteins but could not be trimmed as it lacks a functional GI. As expected, Δ*gls1-S* mutants only displayed G3M9 LLO structures, the same as *WT* cells (Fig. 4*C*).

Mutation in alg10$^+$ gene significantly improves the growth and morphological defects of S. pombe GI mutants

As the LLO pattern produced by Δ*gls1-H* mutants resembled that present in Δ*alg10* mutants (16), we compared the sequence of the *alg10*$^+$ gene in Δ*gls1-S* and Δ*gls1-H* strains. We obtained the whole *alg10* gene (including introns and 5′ and 3′ UTR regions) by PCR from genomic DNA extracted from *WT* and both Δ*gls1* mutants using a high-fidelity polymerase. Upon DNA sequencing, we found an insertion of a thymidine at position 477 from the start codon in the *alg10* gene obtained from Δ*gls1-H* DNA. The mutation was absent in *alg10*$^+$ sequences obtained from *WT* and Δ*gls1-S* DNAs, which were identical to the annotated sequence in the PomBase database (Fig. 5*A*) (17, 18). The insertion in mutant Δ*gls1-H* produces a sequence frameshift that results in a premature stop codon. A 183-amino acid protein was then probably synthesized instead of the 445-amino acid normal one. This confirms that in the mutant with the healthier phenotype an additional mutation in gene *alg10*$^+$ had arisen spontaneously. As in mutant Δ*gls1-H,* a very small amount of G3M9 LLO is still formed (Fig. 4*B*), and the mutation probably does not completely abolish the *alg10*$^+$ gene product activity.

To confirm that a deletion of *alg10*$^+$ gene can indeed improve most of the growth defects of Δ*gls1-S* mutants, we constructed a *S. pombe* Δ*gls1*/Δ*alg10* double mutant strain by a genetic cross using as parental strains Δ*gls1-S*′ (Δ*gls1-S* strain in which the mating type had been converted to *h*$^-$ to allow mating) (Table 1) and a strain in which the gene *alg10*$^+$ had been deleted (Δ*alg10*). We verified the genotype of the double mutant by antibiotic resistance and by PCR (Fig. S1). We then

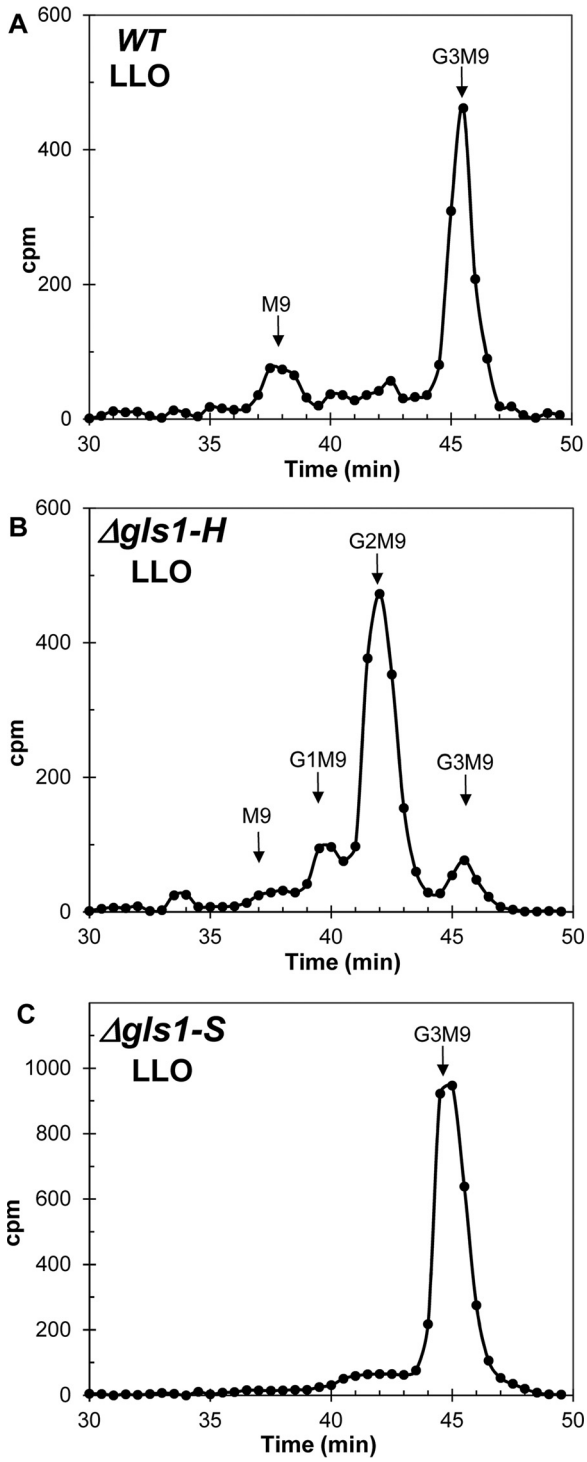

Figure 4. Dol-PP-linked oligosaccharide (LLO) *in vivo* synthesized by *S. pombe* mutants. *WT* (*A*), Δ*gls1-H* (*B*), and Δ*gls1-H* (*C*) exponentially growing mutant cells were labeled with [^{14}C]Glc for 15 min in the presence of cycloheximide and puromycin. Glycans obtained by mild acid hydrolysis were analyzed by paper chromatography in 1-propanol/nitromethane/water (5:2:4), eluted and further solved by HPLC. Positions of standards are indicated by *arrows*.

compared the growth rate in rich medium of the double mutant with that of *WT* and single Δ*alg10*, Δ*gls1-S,* and Δ*gls1-H* mutants. The Δ*gls1/*Δ*alg10* double mutant showed a growth curve very similar to that of the single mutant Δ*gls1-H*, with all its growing parameters significantly improved compared with those of Δ*gls1-S* strain: a shorter lag time, a duplication time at the mid-exponential phase more than twice faster than that of the Δ*gls1-S* strain, and a maximum OD at 600 nm that was about 65% that of the *WT* strain (Fig. 5*B*, Fig. S2, and Table S1). However, the *WT* or Δ*alg10* mutant strain growth parameters were not completely restored.

The aberrant morphology observed in Δ*gls1-S* yeast mutants was also restored to a much normal one when an additional mutation in its *alg10*$^+$ gene was introduced (Fig. S3). Although Δ*gls1-S* strain cultures had mostly small-rounded cells, the Δ*gls1-H* and Δ*gls1/*Δ*alg10* mutants had rod-shaped cells similar to *WT* and Δ*alg10* cells, although still a bit shorter. To quantify the improvement, we calculated the average cell length of the Δ*gls1/*Δ*alg10* double mutant in liquid culture and compared it with those of *WT*, Δ*alg10*, and Δ*gls1* strains. Length measurements of Δ*gls1/*Δ*alg10*, *WT*, Δ*alg10,* and Δ*gls1* cells indicated that the double mutant significantly increased its length with respect to the Δ*gls1-S* ones and that there were no statistically significant differences between Δ*gls1-H* and Δ*gls1/*Δ*alg10* cells (Fig. 5*C*). Taken together, these results indicate that the Δ*gls1* defects were suppressed or at least significantly improved by a simultaneous mutation in the *alg10*$^+$ gene.

As Δ*gls1-H* arose spontaneously as a suppressor mutant during meiosis and spore formation, we wondered whether suppression was also a survival strategy during vegetative growth. We grew Δ*gls1-S* mutants up to stationary phase and initiated a new culture at least five times. Comparison of the growth rate of the resulting culture with that of Δ*gls1-H* mutants suggested that defects in the "true" Δ*gls1* mutants are so severe that cells tend to revert by suppression after several passages, as reverted Δ*gls1-S* (Δ*gls1-S-R*) and Δ*gls1-H* cells showed the same growth rates (Fig. 5*D*).

Lack of G3M9 NLO deglucosylation and not the absence of GI is the main cause of the sick phenotype of Δgls1 cells

Results reported above indicate that mutation of GI-encoding gene produces a very sick phenotype, that the mutant is unable to process G3M9 NLO, and that its growth defects can be at least partially suppressed by a simultaneous mutation in the *alg10*$^+$ gene. A mutation in the *alg10*$^+$ gene is expected to result in the accumulation of G2M9 LLO in the ER membrane, which eventually may be transferred to proteins by OST, although maybe less efficiently than G3M9. Therefore, we determined the LLO and the NLO patterns produced *in vivo* by Δ*gls1/*Δ*alg10 S. pombe* double mutants (Fig. 6). The LLO pattern showed that the main LLO produced *in vivo* was G2M9, plus a small amount of G1M9. This LLO pattern was similar to that produced by the Δ*gls1-H* strain except for the total absence of G3M9 in the double mutant. This result was consistent with a complete absence of alg10p activity (compare Fig. 6*A* with 4*C*). Accordingly, no G3M9 NLO was observed in Δ*gls1/*Δ*alg10* mutants, even though these cells lack GI (Fig. 6*B*). Moreover, almost all NLOs were M9, suggesting that GII had trimmed efficiently the middle and innermost glucoses of the transferred G2M9 glycans. The largest NLO detected was G2M9 upon addition of glucosidase inhibitors (CST and NM-DNJ), thus indicating

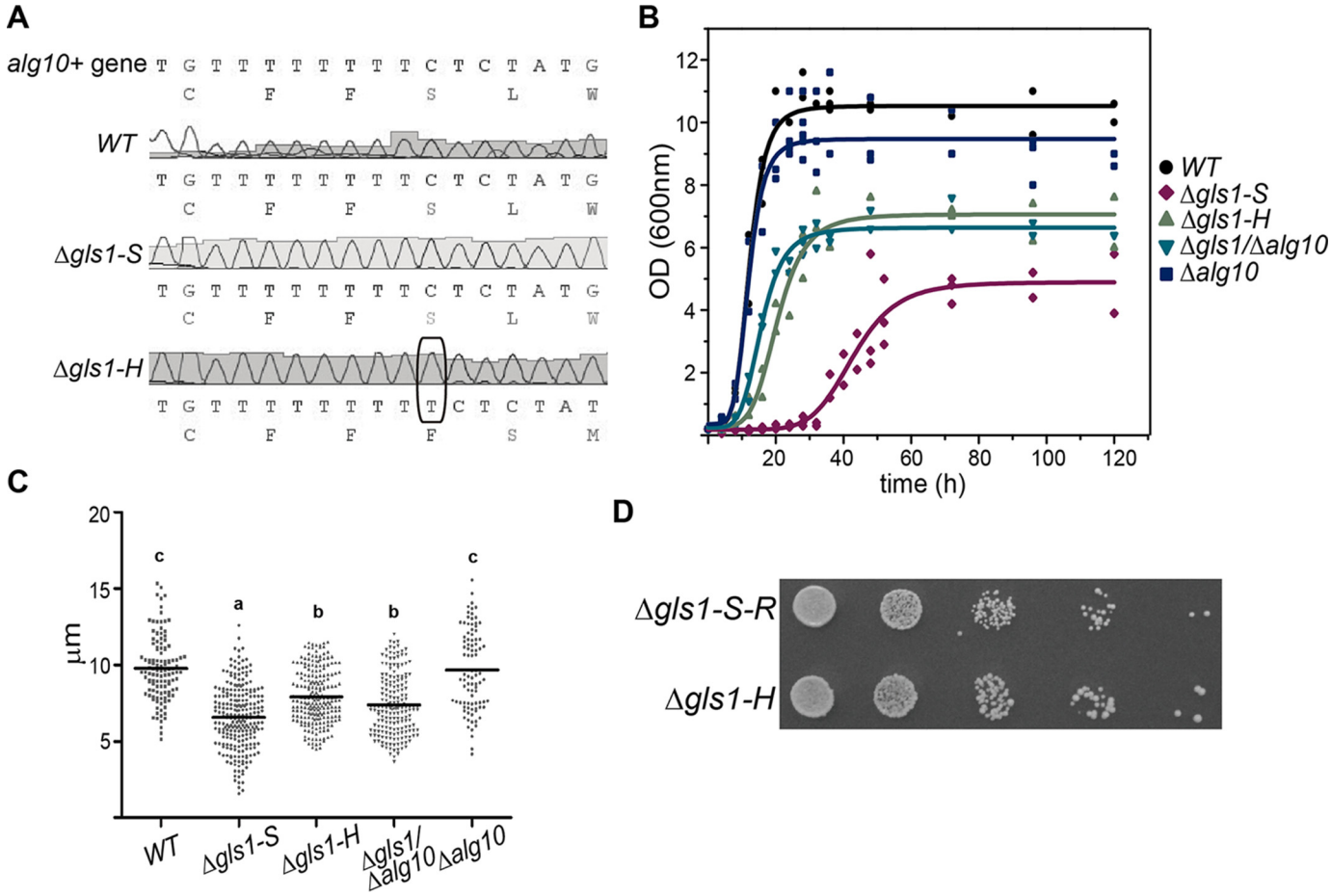

Figure 5. Mutation in *alg10*$^+$ gene suppresses the growth defects of Δ*gls1-S* mutants. *A,* sequence profile of *alg10* gene in Δ*gls1-S* and Δ*gls1-H* mutants. The complete *alg10* gene was obtained by PCR from genomic DNA purified from *WT* and both Δ*gls1* mutants. The products were sequenced and compared with the annotated sequence in PomBase. *B,* growth profile of *S. pombe* mutant strains in liquid-rich YES media. Triplicate cultures of each plotted mutant were started at $A_{600\ nm}$ = 0.2 and grown at 28 °C for 5 days. Aliquots were taken every 4 h and plotted. Data were analyzed using R software. *C,* morphology of *WT*, Δ*alg10,* and Δ*gls1* mutants. Cells were grown in liquid media to an $A_{600\ nm}$ = 1 and photographed with a bright field microscope. Cell lengths (at least 180 for each culture) were measured using ImageJ software. Statistical analyses were done using one-way ANOVA and Bonferroni's multiple comparison tests. Different letters (*a–c*) indicate statistically significant ($p < 0.0001$) differences. *D,* reversion of the growth defect in Δ*gls1-S* mutants after several passages. Δ*gls1-S* and Δ*gls1-H* mutants were grown in liquid YES media until saturation, diluted 1:100 in fresh media, and grown again several times. Finally 5 μl of 10-fold serial dilutions of the cultures were plated in solid-rich media and grown for 72 h at 28 °C. Δ*gls1-S-R* states for the reverted Δ*gls1-S* strain after several passages.

Table 1

***S. pombe* strains used in this work**

Strain (nickname)	Genotype	Origin
ADm (*WT*)	*h*$^-$, *ade6-M210, leu1-32, ura4-D18*	Our stock (31)
Δ*gls1::KanMX*/+ diploid	*h*$^+$/*h*$^+$, *ade6-M210/ade6-M216, leu1-32/leu1-32, ura4-D18/ura4-D18,* Δ*gls1::KanMX*/+	Bioneer
Δ*gls1::NatMX*/+ diploid	*h*$^+$/*h*$^+$, *ade6-M210/ade6-M216, leu1-32/leu1-32, ura4-D18/ura4-D18,* Δ*gls1::NatMX*/+	This work
ΔGI-10A (Δ*gls1-S*)	*h*$^+$, *leu1-32, ade6-M216, ura4-D18,* Δ*gls1::NatMX4*	This work
ΔGI-10D (Δ*gls1-H*)	*h*$^+$, *leu1-32, ade6-M216, ura4-D18,* Δ*gls1::NatMX4*	This work
ΔGI-210m1A (Δ*gls1-S′*)	*h*$^-$, *leu1-32, ade6-M210, ura4-D18,* Δ*gls1::NatMX4*	This work
SPAC56F8.06c (Δ*alg10*)	*h*$^+$, *leu1-32, ade6-M216 ,ura4-D18,* Δ*alg10::KanMX4*	Bioneer
ΔGIA10–18 (Δ*gls1/*Δ*alg10*)	*h*$^+$, *leu1-32, ade6-M210, ura4-D18,* Δ*gls1::NatMX4,* Δ*alg10::KanMX4*	This work
Sp61IIα (Δ*gls2α*)	*h*$^-$, *leu1-32, ade6-M210, ura4-D18, ade1,* Δ*gls2α::ura4*$^+$	Our stock (43)
SpAC227.11c (Δ*yos9*)	*h*$^+$, *leu1-32, ade6-M210, ura4-D18,* Δ*yos9::KanMX6*	Bioneer
Sp61A (Δ*alg6*)	*h*$^-$, *leu1-32, ade1, ade6-M210, ura4-D18,* Δ*alg6::ura4*$^+$	Our stock (45)

that such a structure was the one transferred in Δ*gls1/*Δ*alg10* mutants (Fig. 6*C*).

Our results confirm that cells with a mutation in *alg10*$^+$ genes transfer glycans with the structure G2M9 to proteins and that such defect can suppress the sick phenotype observed in mutants lacking GI. Results also indicate that the presence of triglucosylated glycans in proteins is probably the cause of the severe growth defects observed in the "true" Δ*gls1-S* mutant cells. The fact that the phenotype of the Δ*gls1/*Δ*alg10* double mutant is so similar to that of Δ*gls1-H* strain would suggest that the amount of G3M9 produced by the last strain is too small to produce the toxicity observed in Δ*gls1-S* strain. Our results do not rule out, however, the possibility that GI plays an additional role in the ER, as bypassing its necessity for further glycan processing by simultaneously mutating the *alg10* gene did not fully restore the *WT* phenotype.

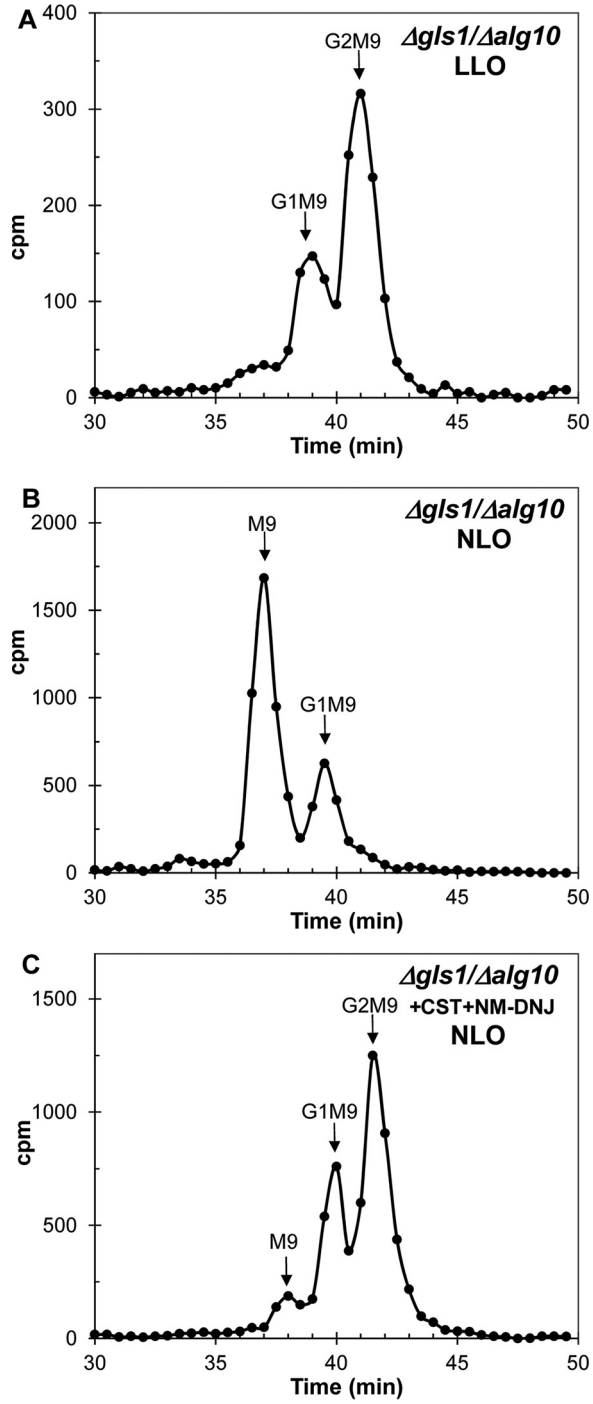

Figure 6. NLOs and LLOs produced by *S. pombe* Δ*gls1*/Δ*alg10* double mutant. Cells were labeled *in vivo* with [^{14}C]Glc for 15 min. NLOs and LLOs were purified and analyzed by paper chromatography in 1-propanol/nitromethane/water (5:2:4), eluted, and further resolved by HPLC. Positions of standards are indicated by *arrows*.

Sick phenotype of Δgls1-S mutants is not due to the impossibility of their glycoproteins to interact with CNX or enter quality control cycles in the ER

Cellular effects produced in Δ*gls1-S* mutants could be due to the lack of interaction of their triglucosylated glycoproteins with CNX. To test whether the absence of lectin–glycoprotein interactions could be the cause of the sick phenotype observed in Δ*gls1-S* mutants, we compared the growth rates of *WT*, Δ*gls1-S,* and Δ*gls2α* mutant cells. As the last ones lack the GII catalytic subunit, they are unable to deglucosylate G2M9 glycans and, the same as in Δ*gls1-S* cells, their glycoproteins cannot interact with CNX. However, Δ*gls2α S. pombe* mutants grew normally when compared with *WT* cells and much better than Δ*gls1-S* mutants (Fig. 7). These results indicate that the absence of CNX–glycoprotein interaction does not affect growth rate and therefore cannot be the cause of the sick phenotype observed in Δ*gls1-S* mutants.

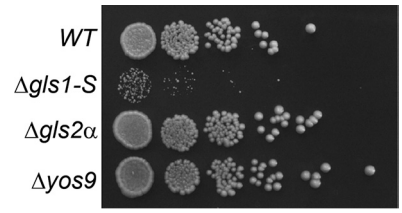

Figure 7. Comparison of the growth phenotype of Δ*gls1-S* cells with those of *S. pombe* mutants whose glycoproteins are unable to interact with CNX or display a defective ERAD pathway. *WT* and the indicated mutant cells were grown up to $A_{600\ nm}$ = 1, and drops (5 μl) of 10-fold dilutions were plated on YES. Plates were incubated for 72 h at 28 °C.

S. pombe cells that lack key components of the ERAD machinery grow normally

OS9 (Yos9p in yeasts), a key component of the ERAD machinery, is a lectin that upon recognition of ER-demannosylated glycans drives irreparably misfolded glycoproteins to proteasomal degradation (Fig. 1*B*). Mutants lacking Yos9p substantially delay misfolded glycoprotein degradation (19, 20). We hypothesized that if irreversibly misfolded glycoproteins bearing three Glc moieties in Δ*gls1-S* cells were not demannosylated in the ER or were not recognized by Yos9p, then *S. pombe* Δ*yos9* mutants would present growth defects similar to those in Δ*gls1-S* cells. Comparison of yeast *WT*, Δ*yos9,* and Δ*gls1-S* mutant cell growth rates indicated that a limitation in the degradation of misfolded glycoproteins did not result in noticeable growth defects (Fig. 7).

OST transfer activity is not significantly inhibited in cells unable to deglucosylate G3M9 NLOs

Our results point to the accumulation of triglucosylated NLOs to be responsible for the severe defects observed in Δ*gls1-S* yeast cells. Such accumulation could inhibit the OST complex, as those glycans are the product of its transfer reaction, thus reducing the glycan-transfer rate. Therefore, this would result in a protein hypoglycosylation similar to that observed when the *N*-glycosylation inhibitor tunicamycin is added to cells (21). To test this hypothesis, we analyzed whether protein hypoglycosylation occurred in *S. pombe* Δ*gls1* mutants. We tested the glycosylation status of CNX, a resident ER glycoprotein with a single glycosylation site, that at nearly stationary phase normally presents soluble and membrane-bound isoforms (22). Upon treatment of cell extracts with Endo H, membrane CNX isoform of all strains tested (*WT*, Δ*gls1-S,* Δ*gls1-H,* Δ*gls1*/Δ*alg10,* and Δ*alg10*) showed an ~2-kDa faster migrating band (Fig. 8*A*). Only Δ*alg10,* Δ*gls1-H,* and Δ*gls1*/Δ*alg10* mutants showed a hypoglycosylation pattern, with a double band corresponding to glycosylated and nonglycosylated CNX

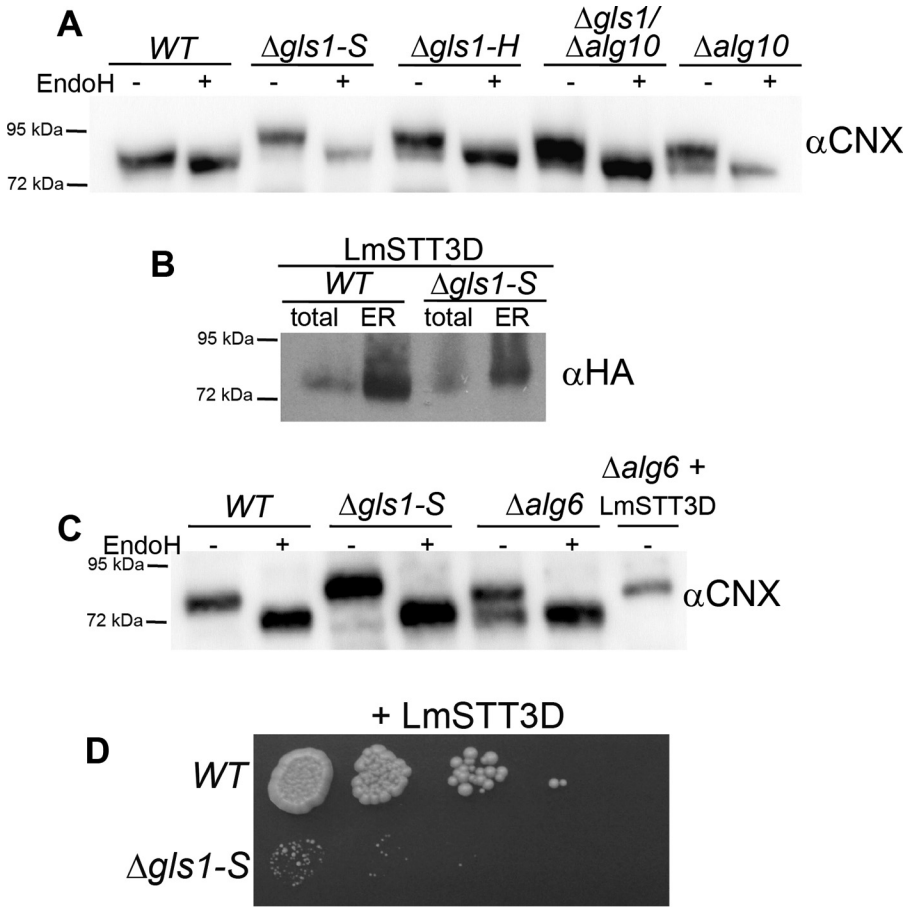

Figure 8. OST protein glycosylation activity is not affected in Δ*gls1-S* mutants. *A,* glycosylation status of CNX in *S. pombe* Δ*gls1* mutants. Cell extracts were prepared from *S. pombe* cultures grown up to $A_{600\ nm} = 1$, treated or not with Endo H, solved by SDS-PAGE 12%, and analyzed by Western blotting using rabbit anti CNX serum 1:10,000 as primary antibody and anti-rabbit HRP 1:30,000 as secondary antibody. *B,* expression of *L. major* STT3D in *S. pombe* mutants. *WT* or Δ*gls1-S* mutants were transformed with HA-epitope–tagged *L. major* STT3D. Total-cell extracts and ER-enriched fractions were obtained, and 50 μg of each submitted to a 12% SDS-PAGE followed by immunoblot using rat anti-HA 1:5000 (Roche Applied Science) followed by anti-rat conjugated to HRP 1:5000 (Sigma). *C,* reversion of CNX hypoglycosylation in Δ*alg6* mutants expressing *L. major* STT3D. Cell extracts were prepared from the indicated *S. pombe* strains and analyzed as in *A*. *D, L. major* STT3D overexpression does not suppress Δ*gls1-S* growth defect. *WT* or Δ*gls1-S* mutants transformed with *L. major* STT3 were grown in EMM medium supplemented with adenine and uracil up to $A_{600\ nm} = 1$. Drops (5 μl) of 10-fold dilutions were plated on solid MMAU an incubated for 72 h at 28 °C.

in the absence of Endo H treatment. No double band was observed in the Δ*gls1-S* mutants in the absence of Endo H, thus indicating that CNX was originally fully glycosylated in Δ*gls1-S* mutants and that the OST ability to transfer pre-assembled glycans to proteins was not affected in that strain (Fig. 8*A*).

The possibility remained, however, that other glycoproteins different from CNX had affected their glycosylation degree by OST in the Δ*gls1-S* mutant. We reasoned that if this were the case, OST overexpression in that mutant would relieve the hypoglycosylation that may occur in any ER glycoprotein. Mammalian and yeast OST are multisubunit complexes whose catalytic subunit is STT3 (23). We expressed *Leishmania major* STT3D, a single-subunit OST of broad-range specificity (24). This OST would not be inhibited by the accumulation of triglucosylated proteins as its natural substrate is M7, the main glycan transferred in those parasites (25). The protein was expressed correctly in the ER, as its expression was enriched in microsomes when compared with total-cell extracts (Fig. 8*B*). Moreover, *L. major* STT3D was able to correct CNX hypoglycosylation observed in an Δ*alg6* mutant (Alg6p is the glycosyltransferase responsible of the addition of the first Glc in G3M9 LLO synthesis, and its absence results in M9 transfer to proteins and in a severe protein hypoglycosylation) (Fig. 8*C*) (26). However, no changes in the growth defects of Δ*gls1-S* were observed upon *L. major* STT3D expression in this strain (Fig. 8*D*). This suggests that an inhibition of the *N*-glycosylation reaction is not the cause of the phenotypic defects observed in the Δ*gls1-S* mutants.

Persistence of three Glc units in the transferred glycan neither precludes glycoprotein extension in the Golgi nor affects S. pombe cell-wall monosaccharide composition

We wondered whether the continued presence of Glc residues in the arm A of the glycan could preclude glycan extension with Man and Gal residues in the Golgi, thus reducing the size of protein-linked galactomannans at the cell surface or somehow affecting cell-wall synthesis. We compared the size of NLOs produced by mutant Δ*gls1-S* that conserved triglucosylated glycoproteins with that of Δ*gls2α* mutant, which displayed instead diglucosylated glycoproteins. We labeled cells with [^{14}C]Glc for 45 min in the absence of DTT, chased them with Glc for 150 min, and isolated NLOs from total-cell glycopro-

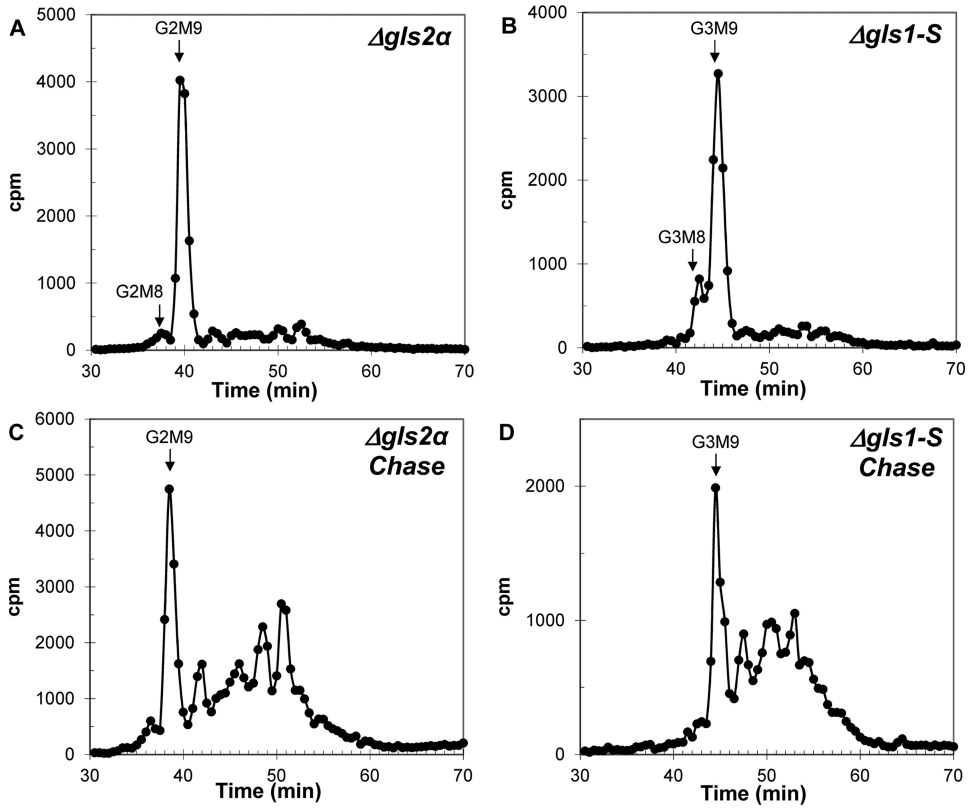

Figure 9. Glycan extension of glycoproteins in *S. pombe* mutants lacking either GI or GII. Cultures of *S. pombe* mutants Δ*gls2α* (*A* and *C*) or Δ*gls1-S* (*B* and *D*) were labeled for 45 min with 5 mM Glc in the presence of 300 μCi/ml [^{14}C]Glc (*C* and *D*) and chased for 150 min with 100 mM Glc. NLOs were purified and analyzed by paper chromatography in 1-propanol/nitromethane/water (5:2:4), eluted, and further solved by HPLC. Positions of standards are indicated by *arrows*.

teins. As expected, after 45 min labeling NLOs obtained from Δ*gls2α* mutants were mainly G2M9 and those obtained from Δ*gls1-S* were G3M9, consistent with the absence of GII and GI activities in the ER, respectively. After 150 min chase, both mutants were able to extend their NLOs in the secretory pathway, and almost no differences were observed between GI- and GII-lacking mutant patterns (Fig. 9). Moreover, the cell wall polysaccharide composition of both mutants was indistinguishable from each other (Fig. S4) and from that of *WT* cells (27) as they produced mainly Glc, but also Man and Gal. As growth rate differences between both strains are evident (Fig. 7), these results indicate that the impossibility of trimming Glc units in the ER did not preclude NLO elongation and that it is not the main cause of the growth impairment of Δ*gls1-S* cells.

Cells lacking GI exhibit a thick cell wall and lack a visible underlying ER

It has been reported that *S. cerevisiae* mutants in the OST catalytic subunit STT3 exhibit a diffused cell wall with loss of the outer mannoprotein layer (28). Transmission electron microscopy (TEM) of *WT*, Δ*gls1-S*, and Δ*gls2α* mutants showed that the cell wall of Δ*gls1-S* is thicker than the others, has a feathered appearance, and lacks the characteristic three-layered structure typical of *WT* cells (Fig. 10, *A–C*) (29). Quantification of the electron-density profiles (Fig. 10, *D–F*) was shown to be relatively homogeneous in the Δ*gls1-S* mutant. This result correlates with the diffuse appearance of its cell wall. Interestingly, this profile appears to be specific for cells lacking GI and bearing triglucosylated glycoproteins, as cells lacking GII and thus bearing diglucosylated glycoproteins display a cell wall identical to that of *WT* cells. Moreover, TEM comparison of ER structures localized below the plasma membrane of *WT*, Δ*gls1-S*, and Δ*gls2α* mutants showed a defined ER structure in the *WT* and Δ*gls2α* strains that was absent in Δ*gls1-S* mutants, thus suggesting that the ER structure may be altered or distorted in the last strain or that the contact sites between the ER and the plasma membrane are lost (Fig. 10, *A–C*).

Continued presence of triglucosylated glycoproteins results in cell death

To understand the severe growth defect in cells unable to remove the glucoses from NLOs, we wondered whether there was a loss of viability at a particular phase in the fission yeast growth curve. Dead cells or cells with a reduced metabolism cannot efficiently exclude the fluorescent dye phloxine B (Fig. S5*A*). We thus analyzed the ability of individual *S. pombe* cells of *WT*, Δ*gls1-S*, Δ*gls1-H*, Δ*gls1*/Δ*alg10*, and Δ*alg10* cultures to exclude phloxine B by flow cytometry (Fig. S5*B*), and we calculated the proportion of cells excluding it at all phases of the growth curve (Fig. 11*A*). The proportion of live and metabolically active cells in Δ*gls1-S* cultures was markedly reduced at all growth phases when compared with that in *WT* ones ($p < 0.001$). Δ*gls1-S* cell viability reached its maximum at the exponential phase, but the value did not exceed 30% that of *WT* cells. The proportion of live cells in Δ*gls1-S* cultures dramatically dropped in the stationary phase. On the contrary,

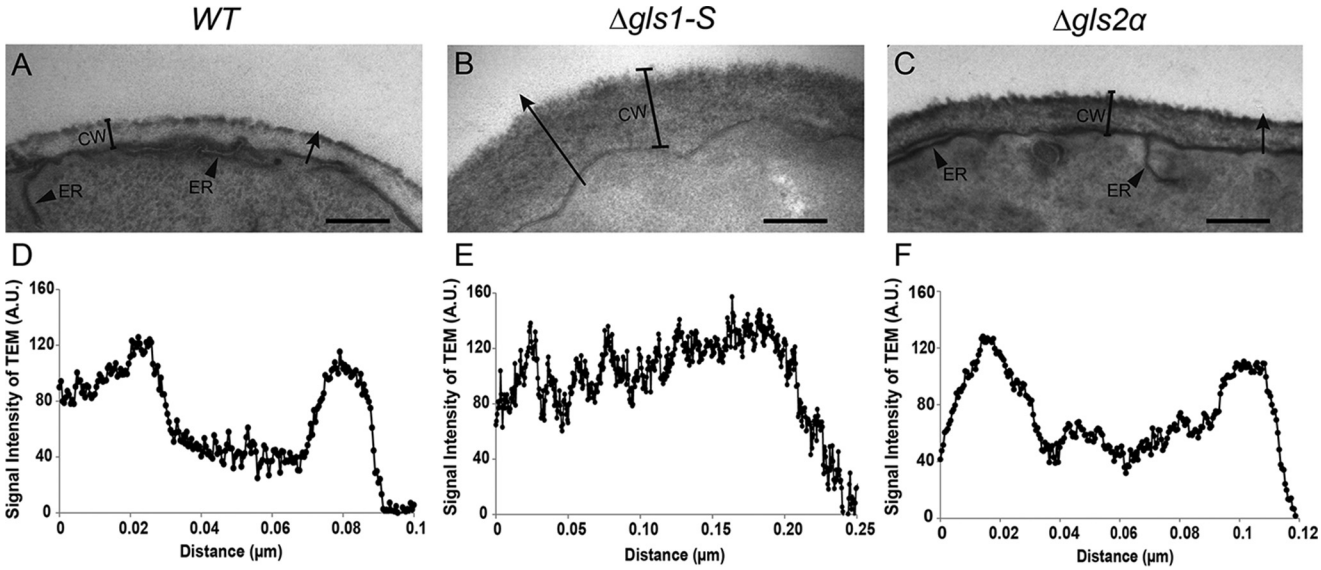

Figure 10. Δ*gls1-S* mutants exhibit changes in the cell wall and in the underlying ER structures. *A–C,* transmission electron microscopy images of *S. pombe WT* (*A*), Δ*gls1-S* (*B*), and Δ*gls2α* (*C*) mutants. Cells were grown to $A_{600\ nm} = 1$ (± 0.2) and fixed with 2.5% glutaraldehyde in 0.1 M PBS supplemented with ruthenium red. The cell wall (*CW*) is indicated with a *bracket* and its underlying ER with an *arrowhead*. The *arrows* in *A–C* correspond to sections used to measure TEM signal intensities (*bar,* 0.1 μm). *D–F,* representative intensity profiles of a *WT* (*D*), Δ*gls1-S* (*E*), and Δ*gls2α* (*F*) *S. pombe* cell wall TEM images. Nine cells for each genotype were analyzed, and three cross-section intensity profiles per cell were plotted, showing an identical behavior. *D–F,* displayed are the characteristic profiles obtained from sections indicated by the *arrows* in *A–C*, respectively. *A.U.*, arbitrary units.

Δ*gls1-H* and Δ*gls1/*Δ*alg10* mutants showed a proportion of metabolically active cells that was significantly higher than the Δ*gls1-S* ones ($p < 0.05$) at all stages of the growth curve. They were 45–60% (Δ*gls1-H*) and 30–50% (Δ*gls1/*Δ*alg10*) that of *WT* cell values (Fig. 11*A*). Results obtained using the exclusion of a vital dye as an indication of vital activity were compared with the ability to generate new colonies (% CFU) of each strain's cells (Fig. 11*B*). The CFU percentage values were reduced at all stages in the Δ*gls1-S* strain. The decrease was especially severe at the stationary phase. Conversely, the Δ*gls1-H* and Δ*gls1/*Δ*alg10* mutant CFU percentage values were quite similar to those of *WT* cells, and this fact was consistent with the observed suppressed phenotype of the mutants.

Expression of human endomannosidase relieves the Δgls1-S mutant sick phenotype

Mammalian cells display an endomannosidase in the Golgi whose expression levels are enhanced in MOGS-CDG patients (13). The enzyme cleaves the bond between Man *f* and Man *g* (Fig. 1*A*) provided either one, two, or three Glc units are present in the glycan (30). In addition to protein-linked M8, it yields $Glc_{1-3}Man$ depending on the substrate hydrolyzed. Although about 80% of glycans in MOGS-CDG patients are then normally processed in the Golgi, they still present a very sick pathology. As *S. pombe* lacks any endomannosidase activity, we expressed human endomannosidase (hEM) as a GFP fusion (*schematized* in Fig. 12*A*) in *S. pombe* Δ*gls1-S* and Δ*gls2α* mutants. The GFP-hEM clone was active in *S. pombe* as microsomes obtained from the transformed Δ*gls2α* strain were able to release a disaccharide from glucose-labeled G1M9 (Fig. 12*B*). The rationale for the use of cells lacking GII to test for endomannosidase activity was to prevent removal of the single Glc from such substrate, in addition to the disaccharide Glc-Man, a fact that would obscure results (Fig. 1*A*). The active hEM expressed in both Δ*gls1-S* and Δ*gls2α* mutants presented a typical Golgi pattern localization for fission yeasts when observed by confocal microscopy (Fig. 12*C*). Those GFP-fluorescent membrane vesicle-like structures distributed within the cell did not correspond to endocytic or degradation vesicles as they did not co-localize with the endocytic pathway-specific dye FM464 (Fig. 12*C*). We then compared the growth rate of Δ*gls1-S* mutants expressing hEM with those of cells transformed with WT $gls1^+$ or with an empty vector. Results obtained showed that expression of hEM in the Golgi of Δ*gls1-S* mutants significantly relieved the sick phenotype but not as well as expression of WT GI (Fig. 12*D*).

Discussion

In an attempt to understand the molecular basis of the pathology observed in individuals with mutations in the GI-encoding gene and thus bearing MOGS-CDG (also known as CDG-IIb), we reproduced in the fission yeast *S. pombe* the genetic defect of the disease. We obtained two mutants: Δ*gls1*-S mutant had a severe growth defect and an aberrant morphology, and Δ*gls1-H* mutant had an almost normal phenotype (Fig. 2). We characterized the NLOs of both strains, and surprisingly, in the healthier Δ*gls1-H* cells most of the NLOs were fully trimmed M9 species (Fig. 3). We speculated that these NLOs could have been formed upon GII deglucosylation of an incomplete glycan transferred to proteins. Analysis of LLOs present in the Δ*gls1-H* strain showed that G2M9 was the main species (Fig. 4*B*). This indicated that the LLO had not reached the complete G3M9 structure, so we speculated that a suppressing mutation had arisen in the enzyme Alg10p responsible for the addition of the outermost glucose to the LLO (Fig. 1). The sequence of *alg10* gene in Δ*gls1-H* mutants showed indeed an insertion that produced a frameshift in the coding sequence

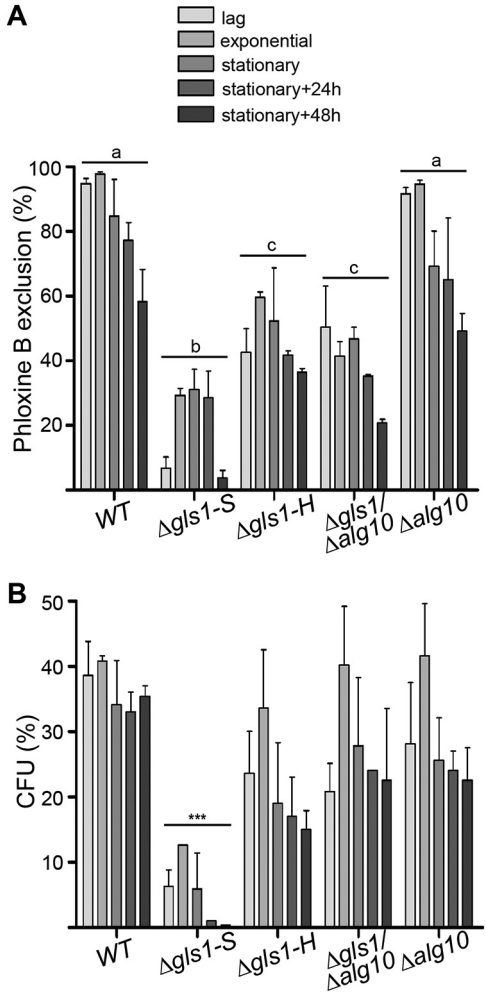

Figure 11. Viability of *S. pombe* mutants at different phases of the growth curve. *A,* percentage of cells able to exclude the vital dye phloxine B. The indicated cell strains were grown in rich media, and aliquots were taken (triplicates for each growth phase) and incubated with the dye phloxine B. Fluorescence of 10,000 cells of each sample was analyzed by flow cytometry. Each *bar* represents the percentage of fluorescent cells. Mean averages that are significantly different from each other ($p < 0.0001$) are indicated with *different letters* and those that are not ($p > 0.05$) are indicated with the *same letter*. *B,* percentage of *S. pombe* mutant cells able to form a colony at the different growth phases. Cells were grown in YES, and aliquots (triplicates) were taken at the different growth phases, diluted, and plated in YEA. After at least 5 days at 28 °C, colonies were counted. Each *bar* represents the percentage of arisen colonies considering 100% the calculated theoretical number of cells plated ($A_{600\ nm} = 1$ was considered to contain 2.2×10^7 cells/ml). *Asterisks* indicate a significant difference ($p < 0.0001$) of Δ*gls1-S* with respect to all other strains.

(Fig. 5*A*). The growth and morphological defects observed in Δ*gls1*-S mutants were relieved in the double knockout strain Δ*gls1*/Δ*alg10* (Fig. 5, *B* and *C,* and Table S1). Taken together, our results indicate that the slow growth and aberrant morphology observed in the nonsuppressed Δ*gls1-S* mutants were due to lack of ER G3M9 NLO deglucosylation. This metabolic defect is, apparently, extremely deleterious for cells as shown by the difficulty of maintaining an unsuppressed Δ*gls1-S* yeast strain: after several rounds of culture replication, the strain tended to suppress the growth defect and started growing as the healthier Δ*gls1-H* (Fig. 5*D*).

Cellular effects of mutations in GI could be in the ER and/or Golgi and/or cell surface. Our results indicate that the phenotypic defects in Δ*gls1-S* mutants are not likely due to a hindered entrance of glycoproteins into the ER quality control of a glycoprotein-folding mechanism as yeast mutants lacking GII activity (Δ*gls2α* mutants) presented a normal growth rate, although they accumulated protein-linked G2M9 structures also unable to enter into such cycles (Fig. 7) (31). A hypothetical impairment of misfolded triglucosylated glycoproteins to be recognized by the ERAD machinery does not seem to be the problem in Δ*gls1-S* mutants either, as lack of the OS9 lectin (Δ*yos9* mutants), which is a central player in the ERAD process as it recognizes demannosylated misfolded glycoproteins and drives them to proteasomal degradation, did not result in relevant growth defects. It may be speculated that increased amounts of triglucosylated glycoproteins in the ER would result in a reaction product inhibition of the OST, thus leading to a severe glycoprotein hypoglycosylation. This appeared not to be the case either as CNX, an ER resident glycoprotein with a single glycosylation site, did not show detectable amounts of hypoglycosylation in Δ*gls1-S* mutant cells (Fig. 8*A*). The possibility existed, however, that hypoglycosylation of other protein(s) may be responsible for the observed phenotypes. Expression in the ER of Δ*alg6 S. pombe* mutants of *L. major* STT3, a subunit with a broad range of substrate specificity that was able to replace the whole OST complex in *S. cerevisiae* (24, 32), was able to revert the hypoglycosylation produced in such a strain. However, its expression did not result in a reversion of the defects in the Δ*gls1-S* mutants caused by accumulation of G3M9 NLOs (Fig. 8*D*), indicating that either there is no OST reaction product inhibition when G3M9 NLOs are not trimmed or that it is not severe enough to result in the observed toxicity.

We next explored the possibility that the presence of three Glc units could prevent the Golgi extension of protein-linked glycans by addition of Man and Gal. A size comparison of NLOs produced by mutant Δ*gls1-S* with those of Δ*gls2α* mutant showed that both strains were capable of extending their protein-linked glycans (Fig. 9) and had normal cell wall monosaccharide compositions (Fig. S4), even though they have very different growth and morphological phenotypes (Fig. 7). As we evaluated the bulk of cell wall glycoproteins, we cannot exclude the possibility that a particular glycoprotein displaying an essential functionality could be affected in Δ*gls1-S* mutants by an impaired glycan elongation. Studies on the morphology of *WT,* Δ*gls1-S,* and Δ*gls2α* cells by TEM showed an altered cell wall ultrastructure only in Δ*gls1-S* cells, which lacked the three-layered structure present in *WT* and Δ*gls2α* cells (Fig. 10). Interestingly, this phenotype resembles that of *S. cerevisiae* cells bearing mutations in the catalytic subunit of the OST, which exhibit a diffused cell wall with loss of the outer mannoprotein layer present in *WT* cells (28). The *S. pombe* ER structure below the plasma membrane was clearly observed in *WT* and Δ*gls2α* cells by TEM. However, no such structures were ever observed in Δ*gls1-S* mutants. The clear differences observed in ER structures of the strains make attractive the possibility that accumulation of triglucosylated glycoproteins in cells lacking GI somehow alters the secretory pathway subcellular structure. This hypothesis is currently under investigation.

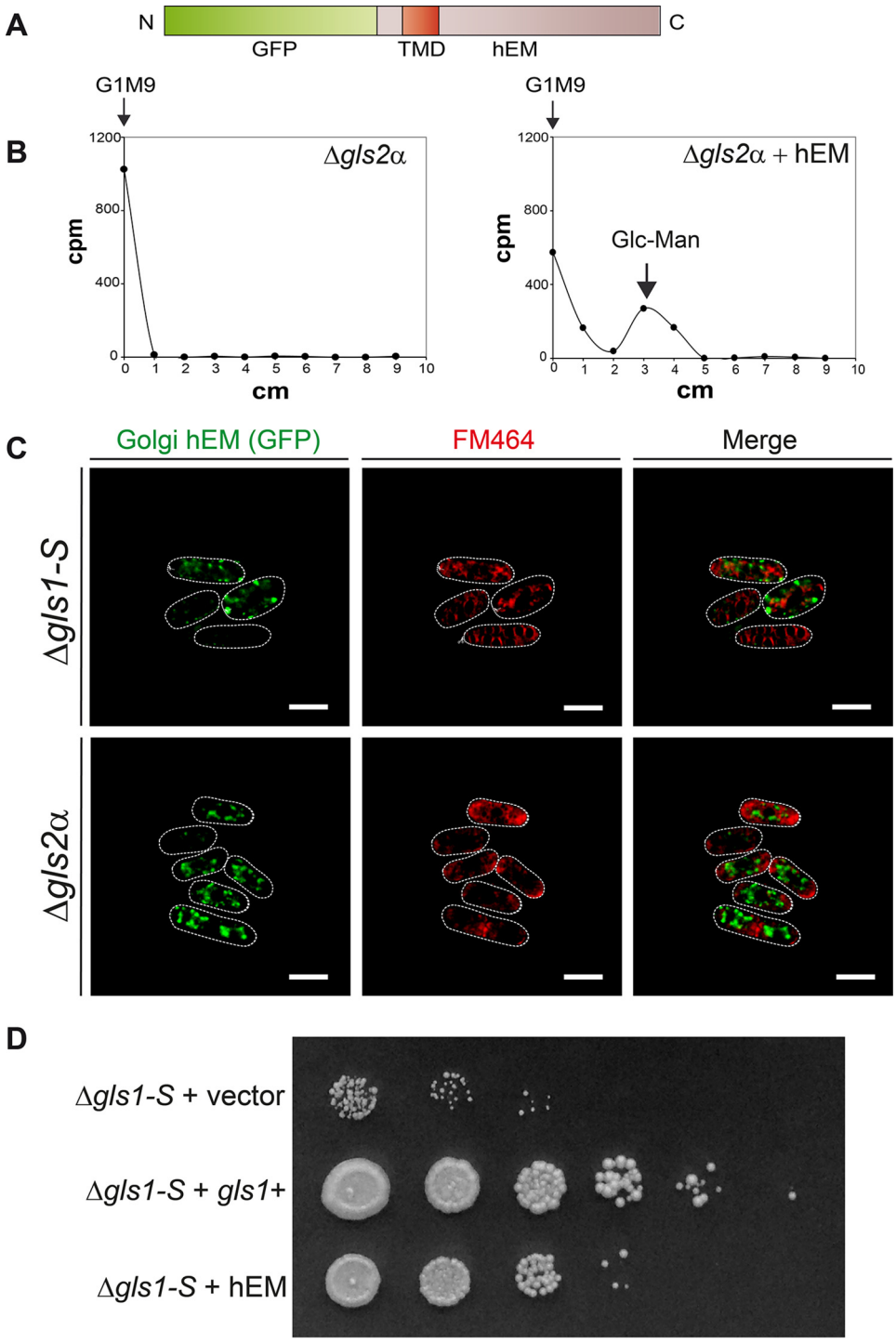

Figure 12. Expressed Golgi human endomannosidase is functional in *S. pombe* and partially rescues the growth defect of Δ*gls1-S* mutants. *A,* schematic representation of the hEM fused to green fluorescent protein (*GFP-hEM*). *TMD*, transmembrane domain. *B,* endomannosidase activity in microsomal fractions of Δ*gls2α S. pombe* mutants. Release of [^{14}C]Glc-Man from 2000 cpm of [^{14}C-Glc]G1M9 was measured using 100 μg of microsomal fractions obtained from Δ*gls2α S. pombe* mutants expressing or not GFP-hEM for 30 min at 37 °C. The reaction was stopped with methanol, and released Glc-Man disaccharides were separated from the substrate on paper chromatography using 2-propanol/acetic acid/H_2O (25:4:9). *C,* GFP-hEM shows a typical Golgi distribution, and it is excluded from endocytic and vacuolar compartments. Confocal images of Δ*gls1-S* and Δ*gls2α* expressing GFP-hEM that were stained with FM4-64 dye were obtained by confocal microscopy using 488 nm argon and 543 nm He-Ne lasers, respectively. *Scale bar,* 5 μm. *D,* relief of the growth defect of Δ*gls1-S* mutants expressing GFP-hEM. Δ*gls1-S* strains transformed either with empty vector, GFP-hEM, or *gls1*$^+$ were grown up to $A_{600\,nm}$ = 1, and drops (5 μl) of 10-fold dilutions were plated on minimal medium lacking leucine. Growth of different strains was compared after a 6-day incubation at 28 °C.

Previous reports showed that *Caenorhabditis elegans* mutants lacking GI did not display any visible morphological or behavioral phenotypes, but life span was greatly reduced (33). We thus investigated whether there was a loss of viability in a particular phase of the fission yeast cell growth curve. With both parameters analyzed, the proportion of cells that exclude the vital fluorescent dye phloxine B and the proportion of cells able to form colony units showed a drastic reduction of viability

at all phases of the growing curve, although the effects were more severe at the early stationary phase (Fig. 11).

Mammalian cells have a Golgi endomannosidase that removes G3M from protein-linked G3M9 (Fig. 1) (34). Expression of the enzyme is enhanced in fibroblasts of patients displaying the MOGS-CDG syndrome thus allowing synthesis of complex type NLOs in the Golgi, more than 80% of which display structures similar to those present in healthy cells (13). Nevertheless, affected individuals still display extremely severe phenotypes. It is unknown whether these are caused by the ~16% of remaining noncanonical NLOs or, alternatively, by the extended occurrence of triglucosylated glycans. Expression of a functional Golgi hEM in the Golgi of Δ*gls1-S* significantly relieved the sick phenotype of the cells, although not as well as expressing GI (Fig. 12). This indicates that the toxic effect exerted by triglucosylated glycoproteins takes place in the Golgi (or ahead in the secretory pathway), that endomannosidase expression has not completely removed the harmful structures, or alternatively, that the extended occurrence of triglucosylated glycoproteins in the ER, the Golgi, and beyond results in growth defects.

In conclusion, we demonstrated that the inability to deglucosylate protein-linked G3M9 glycans in the ER is extremely toxic to the fission yeast. Although we were unable to exactly pinpoint either the cause or the subcellular site of toxicity, we propose that the persistence of those structures may be, at least in part, responsible for the severe pathology observed in MOGS-CDG patients.

Experimental procedures

Materials

Yeast extract and Malt extract were from Britania (Buenos Aires, Argentina). Bactopeptone and yeast nitrogen base (YNB) were from Difco (Detroit, MI). Endo H, protease inhibitors, dithiothreitol (DTT), amino acids, and supplements for culture media were from Sigma. [^{14}C]Glc (301 Ci/mol) was from PerkinElmer Life Sciences. NM-DNJ was from Toronto Biochemicals. Enzymes used for general DNA procedures were from New England Biolabs (Ipswich, MA), and LR clonase was from Invitrogen. Geneticin (G418) was from InVivoGen (Carlsbad, CA), and nourseothricin was from WERNER BioAgents (Jena, Germany).

Strains and media

Escherichia coli DH5α and JA226 were used for cloning purposes and DB3.1 to amplify Gateway plasmids bearing the *ccdB* gene. Bacteria were grown at 37 °C in Luria broth medium (LB: 0.5% NaCl, 1% tryptone, and 0.5% yeast extract), supplemented with 200 μg/ml ampicillin or 50 μg/ml kanamycin as needed. *S. pombe* strains were grown at 28 °C in low adenine-rich media YE (0.5% yeast extract, 3% glucose) when testing for *ade6* genotype or in YES medium (YE medium supplemented with 75 mg/liter adenine). *S. pombe* were selected in EMM minimal medium (35, 36) supplemented with adenine 75 mg/liter, leucine 250 mg/liter, or uracil 75 mg/liter as required. Geneticin was added to YES media at 200 μg/ml for *kanMX* marker selection, and nourseothricin was added to YES media at 100 μg/ml for *NatMX* marker selection. When double selection for geneticin and auxotrophic markers was needed, NH_4Cl was replaced by 0.37% monosodium L-glutamate as the nitrogen source in EMM. Malt extract medium (3% Bacto Malt Extract, pH 5.5, supplemented with adenine, uracil, and leucine) was used for matings. The *S. pombe* strains used in this work are summarized in Table 1.

DNA and cloning procedures

General DNA procedures were as described previously (37). Yeast DNA extraction was performed as described in Ref. 38.

The *alg10*$^+$ gene in *S. pombe WT*, Δ*gls1-H,* and Δ*gls1-S* strains was amplified in two parts using genomic DNA of each strain as a template and the primer pairs alg10 –5′NC (5′-CCAAACTTCCTGCCAACAAC-3′)/alg10rev (5′-CAATCCCCACTTAGCTGAAG-3′) and alg10fw (5′-CTGGCTTGTAGGCGTAATTG-3′tj;1)/alg10 –3′NC (5′-GGTGCTCGTTGATTTTTGGT-3′) in a high-fidelity PCR using KOD (Merck). Both PCR products obtained from each mutant were purified by QIAquick gel extraction kit (Qiagen) and sequenced.

The gateway pDONR201 plasmid containing clone 28/H08 (*S. pombe gls1*$^+$ gene, which was obtained from RIKEN DNA Bank (39)) was transferred to the pREP41-ccdb2 Gateway-compatible *S. pombe* destination expression vector (kindly provided by Dr. M. Yoshida, Chemical Genetics Laboratory, RIKEN DNA Bank, Japan) by the LR recombination reaction (Invitrogen) as indicated by the manufacturer. Recombinant expression plasmid was amplified and recovered from JA226 *E. coli* strain. *S. pombe* competent Δ*gls1-S* cells were then electroporated with the pREP41-GI episomal-replicating constructs and selected in EMM supplemented with adenine and uracil.

L. major STT3D was amplified from plasmid pRS425-STT3D (kindly provided by Dr. Markus Aebi, ETH, Zurich, Switzerland) (24) in-frame with a sequence coding the hemagglutinin (HA) epitope tag using the following primers that provide at both ends the *attB* sites for Gateway recombination: attB1-STT3D fw (5′-GGGGACAAGTTTGTACAAAAAAGCAGGCTGGATGGGCAAGCGGAAGGG-3′) and attB2+stop STT3D rev (5′-GGGGACCACTTTGTACAAGAAAGCTGGGTtcaAGCGTAATCTGGAACGTC-3′). The 2600-bp fragment was introduced in pDONR-201ccdB vector by recombination using BP clonase (Invitrogen) and the plasmids recovered from *DH5α E. coli* strain. Positive clones were identified by colony PCR using primers attb-STT3fw and pDONR201a (5′-CATCAGAGATTTTGAGACAC-3′) and sequenced. The insert was then transferred to a pREP1-ccdB (Riken) (39) destination vector using LR clonase as described above. The resulting expression vector pREP1-STT3D-HA was sequenced and electroporated into *WT* and Δ*gls1-S* yeast cells. Transformants were selected in EMM lacking leucine.

Human Golgi endomannosidase fused to GFP was amplified with KOD polymerase from plasmid pSV-GFP-hEM (34) using primers pREP3X-XhoI-fEGFP (5′-TTCTCACTTTCTGACTTATAGTCGCTTTGTTAAATGGCCTCGAGATGGTGAGCAAGGGCGAGGAG-3) and hEM-SmaI-pREP3x (5′-AACCCTAGCAGTACTGGCAAGGGAGACATTCCTTTTACCCGGGTTAAGAAACAGGCAGCTGGCG-3′) that introduce ~40 bp of flanking homology to *S. pombe* expression vector pREP3X. The insert was cloned by gap repair in *S. pombe*

by transforming competent *WT* cells with 5 μg of the insert plus 1 μg of pREP3X previously opened with SmaI and XhoI restriction enzymes (40, 41). Transformants selected in EMM lacking leucine were screened by colony PCR to detect the presence of plasmid pREP3X-GFP-hEM produced by homologous recombination. Total DNA obtained from positive cells was used to transform *E. coli*, and plasmids were recovered and sequenced (41). The same clone was introduced into Δ*gls1-S* and Δ*gls2α S. pombe* strains.

Genetic procedures

S. pombe transformations by electroporation—*S. pombe* electrocompetent cells were prepared by extensively washing exponentially growing cultures twice with 1 volume of sterile water, twice with 1 M sorbitol, and finally resuspended at a 1:100 of the initial volume in 1 M sorbitol. Plasmidic supercoiled DNA (0.2 μg) or linear DNA (0.5–1 μg) were electroporated at 1.5 kV, 200 ohm, 25 microfarads with a Gene Pulser II (Bio-Rad). Cells were recovered in 0.5 M sorbitol in YES for 1 h at 28 °C, harvested, and plated in the appropriate selective media.

Construction of Δgls1::NatMX haploid strains—The geneticin resistance cassette of the heterozygous Δgls1::KanMX/+ diploid *S. pombe* strain purchased from Bioneer (Korea) was exchanged by the nourseotricine resistance cassette according to Sato *et al.* (42) as follows: primers MD1 (5′-CGGATCCCCGGGTTAATTAAGGCG-3′) and MD2 (5′-GAATTCGAGCTCGTTTAAACACTGGATGGCGGCGTTAGTATCG-3′) were used in a PCR using KOD (Merck) to obtain *NatMX6* (nourseothricin-resistant marker) flanked by promoter P_{TEF} and terminator T_{TEF} using plasmid pCR2.1-Nat as a template (kindly provided by Takashi Toda, London Research Institute, UK). This DNA fragment was gel-purified and used to transform electrocompetent Δ*gls1::KanMX/+* diploid *S. pombe* mutants. Nourseothricin-resistant Δ*gls1::NatMX/+* diploid *S. pombe* colonies were tested for sensitivity to geneticin, and homologous recombination was verified by PCR using primers gls1–5′NC B (5′-GCTCCAAATGTTTTACG CAG-3′) and ClonNAT rev (5′-CGAGACGACCACGAAGC-3′). To obtain haploid Δ*gls1::NatMX* strains, sporulation was induced by transformation of the nourseothricin-resistant diploid strain with plasmid pON177 (Bioneer) according to company instructions followed by selection of uracil phototrophs. Spore micromanipulations were carried out with a Manual Micromanipulator (Singer Instruments Co). Δ*gls1::NatMX* genotypes of the spores were determined by antibiotic resistance and also by colony PCR with the primers ClonNAT fw (5′-CTTCGTGGTCGTCTCGTAC-3) and gls1–3′NC B (5′-AAATACGAAACGCAGTTCGC-3′). Δ*gls1-S* and Δ*gls1-H* haploid nourseothricin mutants were obtained from the dissection of the same tetrad (Table 1).

Construction of S. pombe double mutants—*S. pombe* Δ*alg10* and Δ*yos9* mutants were purchased from Bioneer (Korea). *S. pombe* Δ*gls2α* strain construction was described previously (43). Double mutants were obtained using standard genetic techniques for mating, sporulation, tetrad dissection, and analysis, as described previously (27, 35). Relevant genotypes were determined by antibiotic resistance or auxotrophic growth in the appropriate media and also by colony PCR with the primers described below. To construct ΔGIA10-18 strain, first haploid Δ*gls1-S* was mated with ADm to obtain Δ*GI210m-1A*. This *h*− strain was in turn mated with strain Δ*alg10* (SPAC56F8.06c), and the diploids obtained were sporulated and tetrads dissected by micromanipulation. The genotype of the resulting spores that were both geneticin- and nourseothricin-resistant was confirmed by PCR using the primer pairs ClonNAT fw/gls1–3′NC B for Δ*gls1::NatMX* and Spalg10s 5′NC (5′-CCAAACTTCCTGCCAACAAC-3′)/KanMXrev2 (5′-CGCTACCTTTGCCATGTTTCAG-3′) for Δ*alg10::KanMX*, respectively. Mating types were determined by PCR as described (44).

Analysis of NLO and LLOs synthesized in vivo

S. pombe cultures in exponential growth phase were harvested, extensively washed with 1% YNB medium without glucose, and resuspended in 2 volumes (v/w) of the same medium. For NLO analysis, 0.5 ml of cells were preincubated with the mannosidase inhibitor 3.5 mM kifunensine for 30 min and with 5 mM DTT for 5 min and pulsed for 15 min in 5 mM Glc with 300 μCi/ml [^{14}C]Glc at 28 °C. When GI and GII inhibitors CST and NM-DNJ were used, they were added 60 min prior to labeling at 8.5 and 5 mM, respectively. Purification and protease digestion of glycoproteins and Endo H–sensitive NLO purification were performed as described previously (10). Glycans were run on paper chromatography in Whatman 1 papers and 1-propanol/nitromethane/H_2O (5:2:4) as solvent, and peaks were identified by standards run in parallel. To improve the resolution of the glycan species, the identified glycans were eluted from the papers and resolved by HPLC using a TSK-GEL Amide-80 column (4.6 mm inner diameter × 25 cm; Tosoh Bioscience, Tokyo, Japan) with a mobile phase of H_2O/CH_3CN in a linear gradient from 35:65 to 55:45 over 65 min and a flow rate of 0.75 ml/min at room temperature as reported (45). For the analysis of LLO, 1 ml of washed cells were pulsed for 15 min in 5 mM Glc with 300 μCi/ml [^{14}C]Glc at 28 °C in the presence of 50 μg/ml puromycin and 75 μg/ml cycloheximide. Cells were precipitated with 5 ml of methanol, and the pellet was extracted three times with $CHCl_3$/methanol (3:2). The pellet was then washed once with methanol and once with water, resuspended in 2 ml of water and 1 ml of glass beads, vortexed for 10 min, and centrifuged. The resulting pellet was washed four times with water and then extracted with CH_3CN/methanol/water (1:1:0.3). The extracted material was dried and boiled for 15 min in 1 ml of 0.02 N HCl. Once cold, 3 ml of $CHCl_3$ and 2 ml of methanol were added and centrifuged. The upper phase was recovered, dried, and analyzed as described for NLO.

Analysis of glycan extension in the secretory pathway and cell wall composition of GI and GII mutants

S. pombe cultures in exponential growth phase were harvested and washed with 1% YNB medium without glucose, and the pellet was resuspended in 2 volumes (v/w) of the same medium. Cells (1 ml) were labeled for 45 min in 5 mM Glc with 300 μCi/ml [^{14}C]Glc. Half of each labeled sample was washed with 20 volumes of 1% YNB, centrifuged, and chased for 150 min in 0.5 ml of 1% YNB containing 100 mM glucose, whereas the other half was processed immediately. Glycoprotein purification and glycan pattern analysis of all samples were per-

formed as described above for NLOs. To determine cell wall monosaccharide composition, the water-insoluble material obtained after protease digestion of labeled glycoproteins was heated for 150 min at 100 °C in 2 N NaOH in a final volume of 2.5 ml, precipitated with 3 ml of methanol, and washed three times with 75% methanol. Insoluble material was heated for 4 h at 100 °C in 1 N HCl, dried at room temperature, and submitted to paper chromatography in Whatman 1 paper with butanol/pyridine/H_2O (10:3:3) as solvent.

Purification of total-cell protein extracts, microsomal fractions, and protein deglycosylation

Yeast whole-cell extracts were obtained from 20 ml of exponentially growing cultures at $A_{600\,nm} = 2$. Cells were washed once with water, harvested, and broken with glass beads (0.5 mm inner diameter) by 10 repetitive cycles of 1-min vortexing followed by 1 min on ice in 0.1 M HEPES, pH 7.2, 1% Triton X-100, 5 mM EDTA with protease inhibitors (100 μM phenylmethylsulfonyl fluoride, 10 μM L-1-tosylamido-2-phenylethyl chloromethyl ketone, 10 μM *N-p*-tosyl-L-lysine chloromethyl ketone, 10 μM leupeptin, 10 μM pepstatin, and 10 μM E64), and cleared by centrifugation at 20,000 × *g* for 20 min. Microsomal (ER and Golgi-enriched) fractions were obtained as described previously (31). To measure *S. pombe* endomannosidase activity, Δ*gls2α* microsomal fractions were resuspended in 100 mM phosphate buffer, pH 6.8, 0.25 M sucrose, 1 mM EDTA, and protease inhibitors. Protein concentrations were determined by protein assay as described by Bio-Rad. To obtain deglycosylated extracts, 50 μg of whole-cell proteins were denaturalized with 0.5% SDS and 40 mM DTT at 100 °C, and treated with 1 milliunit of Endo H overnight at 37 °C in 50 mM triethanolamine, pH 5.5.

Endomannosidase activity assays

Endomannosidase activity of 100 μg of total protein from microsomal fractions of *S. pombe* Δ*gls2α* cells was determined by incubation with 2000 cpm of [*glucose*-^{14}C]$Glc_1Man_9GlcNAc$ in 50 μl of 50 mM sodium phosphate buffer, pH 6.8, 0.5% Triton X-100 for 30 min at 37 °C. Reactions were stopped by the addition of 50 μl of methanol, incubated for 5 min at 60 °C, and centrifuged for 5 min at 15,000 × *g*. Released [^{14}C]Glc-Man and the remaining non-hydrolyzed substrate of the supernatant were separated by ascending paper chromatography in Whatman 1 using 2-propanol/acetic acid/H_2O (25:4:9) as solvent. The disaccharide nature of the released radioactivity was confirmed by ascending paper chromatography using 1-butanol/ethanol/H_2O (10:1:2) as solvent and sucrose, maltose, and Glc as standard.

Immunoblottings

Total *S. pombe* proteins (50 μg) were run in SDS-PAGE and electrotransferred to Immobilon-P membranes (Millipore) 1.5 h at 100 mA. For detection of the CNX glycosylation status, the resolving gel was 12%, and the membrane was incubated first with previously obtained rabbit anti-*S. pombe* CNX antibody (1:10,000) (46) and then with anti-rabbit antibody (1:3000) conjugated to HRP (Sigma). For STT3D-HA detection, the gel was 9%, and the membrane was incubated with rat anti-HA (1:5000) (Roche Applied Science) followed by anti-rat conjugated to HRP (1:5000) (Sigma). Bands were revealed using West Pico SuperSignal chemiluminescent substrate (ThermoFisher Scientific, Waltham, MA) following the instructions of the manufacturer. Membranes were developed using an Image Quant Las4000 luminescent image analyzer.

Transmission electron microscopy

WT or Δ*gls1-S* cells were grown to $A_{600\,nm} = 1$ (±0.2) and fixed overnight at room temperature using 2.5% glutaraldehyde in 0.1 M phosphate buffer, pH 7.4, supplemented with 0.01% ruthenium red to increase electronic contrast in the cell wall. This step was followed by post-fixation in 1% osmium tetroxide for 1 h. Samples were stained overnight at 4 °C in 2% uranyl acetate and dehydrated with ethanol. Then they were embedded in Epoxy resin (Durcupan), and 60–70-nm sections were cut. Images were obtained using a transmission electron microscope (TEM-Zeiss-EM109T) and photographed with a Gatan ES1000W digital camera. Images with a ×85,000 magnification of 9–12 cells per genotype were taken randomly. The signal intensities along the cell wall's cross-sections were obtained using ImageJ software.

Subcellular localization of expressed hEM

Δ*gls1-S* or Δ*gls2α* cells transformed with Golgi hEM fused to GFP were grown to $A_{600\,nm} = 1$ in EMM lacking leucine. Cells (200 μl) were harvested and resuspended in 500 μl of YES. Images were obtained using a Zeiss confocal microscope LSM 710, with a ×63 Zeiss Plan-Apochromat objective (NA 1.4). At least 10 images were taken randomly per genotype. For processing images, a smooth filter was set using ImageJ software to improve the quality. For endocytic pathway staining, 20 μl of cultures were incubated with 0.1 mg/ml FM4-64 at 30 °C for 90 min and washed with PBS.

Growth, morphology, and survival of S. pombe mutants

Growth of *S. pombe* mutants in solid media was performed as follows: cultures of to-be-compared strains at the early stationary phase were diluted to a final concentration of 2×10^6 cells/ml. Tenth dilution series in YES were performed, and drops of 5 μl of each dilution were spotted in solid YES, in triplicate. Plates were incubated at 28 °C, and images were taken every 24 h with an Olympus C-610 digital camera for 5 days.

To perform growth curves of *S. pombe* mutants in liquid media, a pre-culture of each *S. pombe* strain at the end of the exponential phase was used to start three 50-ml cultures of YES at $A_{600\,nm} = 0.2$ in 250-ml flasks (time 0), which were grown for 5 days at 28 °C with agitation at 250 rpm. Aliquots were taken every 4 h to monitor OD at 600 nm. Data were analyzed with R (47) and a logistic adjustment was used.

Survival of *S. pombe* mutants at different stages of the growth curve was scored by counting colony-forming units from dilutions of aliquots taken at each time point plated on YES and incubated for 7 days at 28 °C. The proportion of colony formation units in a population was considered as the percentage of survival at a given time point. Cell growth curves were performed in independent triplicates for each mutant. ANOVA statistical analysis was done using Bonferroni's test.

Survival was also measured by the ability to exclude the fluorescent dye phloxine B (disodium 2′,4′,5′,7′-tetrabromo-4,5,6,7-tetrachlorofluorescein) as follows: for each time point of the growing curve 1.4×10^7 cells were incubated in 1 ml of a final volume of YES with 5 μg/ml phloxine B for 2 h at 28 °C with shaking as described (48). An amount of 10,000 cells were then analyzed by flow cytometry using a FACSCalibur flow cytometer (BD Biosciences) with an argon laser (excitation at 488 nm). Emission at 546–550 nm (filter FL2) was monitored for phloxine B–stained cells that were compared with a non-stained culture. As a control of stained death-cell fluorescence intensity, cultures in exponential growth were heated 1 h at 65 °C and analyzed by flow cytometry as described above. ANOVA statistical analysis was done using Bonferroni's test.

To measure the cell length of mutant yeasts, images of cultures in exponential phase ($A_{600\ nm} = 1$) were acquired using an Olympus BX60 light transmission microscope with a UPlanFI ×100 oil objective (NA = 1.30) and an Olympus DP71 camera. Cell lengths (at least 180 for each mutant) were measured with ImageJ software. Statistical analyses were done using Bonferroni's multiple comparison test.

Author contributions—G. L. G., A. P., and C. D. conceptualization; G. L. G. and C. D. data curation; G. L. G. and C. D. formal analysis; G. L. G., A. V., S. I. A., E. E., A. P., and C. D. investigation; G. L. G., A. V., S. I. A., and C. V. methodology; A. P. and C. D. writing-review and editing; C. D. supervision; C. D. funding acquisition; C. D. writing-original draft; C. D. project administration.

Acknowledgments—We thank Dr. Markus Aebi (ETH, Zurich, Switzerland), Dr. Takashi Toda (London Research Institute, United Kingdom), and Dr. M. Yoshida (Chemical Genetics Laboratory, RIKEN DNA Bank, Japan) for providing us with plasmids pRS425-STT3D, pCR2.1-Nat, and pREP41-ccdb2, respectively.

References

1. Aebi, M. (2013) *N*-Linked protein glycosylation in the ER. *Biochim. Biophys. Acta* **1833,** 2430–2437 CrossRef Medline
2. Mohorko, E., Glockshuber, R., and Aebi, M. (2011) Oligosaccharyltransferase: the central enzyme of *N*-linked protein glycosylation. *J. Inherit. Metab. Dis.* **34,** 869–878 CrossRef Medline
3. Parodi, A. J. (2000) Protein glucosylation and its role in protein folding. *Annu. Rev. Biochem.* **69,** 69–93 CrossRef Medline
4. D'Alessio, C., Caramelo, J. J., and Parodi, A. J. (2010) UDP-GlC:glycoprotein glucosyltransferase-glucosidase II, the ying-yang of the ER quality control. *Semin. Cell Dev. Biol.* **21,** 491–499 CrossRef Medline
5. Sousa, M. C., Ferrero-Garcia, M. A., and Parodi, A. J. (1992) Recognition of the oligosaccharide and protein moieties of glycoproteins by the UDP-Glc:glycoprotein glucosyltransferase. *Biochemistry* **31,** 97–105 CrossRef Medline
6. Caramelo, J. J., Castro, O. A., Alonso, L. G., De Prat-Gay, G., and Parodi, A. J. (2003) UDP-Glc:glycoprotein glucosyltransferase recognizes structured and solvent accessible hydrophobic patches in molten globule-like folding intermediates. *Proc. Natl. Acad. Sci. U.S.A.* **100,** 86–91 CrossRef Medline
7. Freeze, H. H., Schachter, H., and Kinoshita, T. (2015) in *Essentials of Glycobiology* (Varki, A., Cummings, R. D., Esko, J. D., Stanley, P., Hart, G. W., Aebi, M., Darvill, A. G., Kinoshita, T., Packer, N. H., Prestegard, J. H., Schnaar, R. L., and Seeberger, P. H., eds) pp. 569–582, Cold Spring Harbor Laboratory Press, Cold Spring Harbor, NY
8. De Praeter, C. M., Gerwig, G. J., Bause, E., Nuytinck, L. K., Vliegenthart, J. F., Breuer, W., Kamerling, J. P., Espeel, M. F., Martin, J. J., De Paepe, A. M., Chan, N. W., Dacremont, G. A., and Van Coster, R. N. (2000) A novel disorder caused by defective biosynthesis of *N*-linked oligosaccharides due to glucosidase I deficiency. *Am. J. Hum. Genet.* **66,** 1744–1756 CrossRef Medline
9. Sadat, M. A., Moir, S., Chun, T. W., Lusso, P., Kaplan, G., Wolfe, L., Memoli, M. J., He, M., Vega, H., Kim, L. J. Y., Huang, Y., Hussein, N., Nievas, E., Mitchell, R., Garofalo, M., *et al.* (2014) Glycosylation, hypogammaglobulinemia, and resistance to viral infections. *N. Engl. J. Med.* **370,** 1615–1625 CrossRef Medline
10. Fernández, F. S., Trombetta, S. E., Hellman, U., and Parodi, A. J. (1994) Purification to homogeneity of UDP-glucose:glycoprotein glucosyltransferase from *Schizosaccharomyces pombe* and apparent absence of the enzyme from *Saccharomyces cerevisiae*. *J. Biol. Chem.* **269,** 30701–30706 Medline
11. Kim, D. U., Hayles, J., Kim, D., Wood, V., Park, H. O., Won, M., Yoo, H. S., Duhig, T., Nam, M., Palmer, G., Han, S., Jeffery, L., Baek, S. T., Lee, H., Shim, Y. S., *et al.* (2010) Analysis of a genome-wide set of gene deletions in the fission yeast *Schizosaccharomyces pombe*. *Nat. Biotechnol.* **28,** 617–623 CrossRef Medline
12. Herscovics, A. (1999) Processing glycosidases of *Saccharomyces cerevisiae*. *Biochim. Biophys. Acta* **1426,** 275–285 CrossRef Medline
13. Völker, C., De Praeter, C. M., Hardt, B., Breuer, W., Kalz-Füller, B., Van Coster, R. N., and Bause, E. (2002) Processing of *N*-linked carbohydrate chains in a patient with glucosidase I deficiency (CDG type IIb). *Glycobiology* **12,** 473–483 CrossRef Medline
14. Piel, M., and Tran, P. T. (2009) Cell shape and cell division in fission yeast. *Curr. Biol.* **19,** R823–R827 CrossRef Medline
15. Hossain, T. J., Harada, Y., Hirayama, H., Tomotake, H., Seko, A., and Suzuki, T. (2016) Structural analysis of free *N*-glycans in α-glucosidase mutants of *Saccharomyces cerevisiae*: lack of the evidence for the occurrence of catabolic α-glucosidase acting on the *N*-glycans. *PLoS One* **11,** e0151891 CrossRef Medline
16. Burda, P., and Aebi, M. (1998) The ALG10 locus of *Saccharomyces cerevisiae* encodes the α-1,2 glucosyltransferase of the endoplasmic reticulum: the terminal glucose of the lipid-linked oligosaccharide is required for efficient *N*-linked glycosylation. *Glycobiology* **8,** 455–462 CrossRef Medline
17. Wood, V., Harris, M. A., McDowall, M. D., Rutherford, K., Vaughan, B. W., Staines, D. M., Aslett, M., Lock, A., Bähler, J., Kersey, P. J., and Oliver, S. G. (2012) PomBase: a comprehensive online resource for fission yeast. *Nucleic Acids Res.* **40,** D695–D699 CrossRef Medline
18. McDowall, M. D., Harris, M. A., Lock, A., Rutherford, K., Staines, D. M., Bähler, J., Kersey, P. J., Oliver, S. G., and Wood, V. (2015) PomBase 2015: updates to the fission yeast database. *Nucleic Acids Res.* **43,** D656–D661 CrossRef Medline
19. Buschhorn, B. A., Kostova, Z., Medicherla, B., and Wolf, D. H. (2004) A genome-wide screen identifies Yos9p as essential for ER-associated degradation of glycoproteins. *FEBS Lett.* **577,** 422–426 CrossRef Medline
20. Szathmary, R., Bielmann, R., Nita-Lazar, M., Burda, P., and Jakob, C. A. (2005) Yos9 protein is essential for degradation of misfolded glycoproteins and may function as lectin in ERAD. *Mol. Cell* **19,** 765–775 CrossRef Medline
21. Fernandez, F., Jannatipour, M., Hellman, U., Rokeach, L. A., and Parodi, A. J. (1996) A new stress protein: synthesis of *Schizosaccharomyces pombe* UDP–Glc:glycoprotein glucosyltransferase mRNA is induced by stress conditions but the enzyme is not essential for cell viability. *EMBO J.* **15,** 705–713 CrossRef Medline
22. Núñez, A., Dulude, D., Jbel, M., and Rokeach, L. A. (2015) Calnexin is essential for survival under nitrogen starvation and stationary phase in *Schizosaccharomyces pombe*. *PLoS One* **10,** e0121059 CrossRef Medline
23. Wild, R., Kowal, J., Eyring, J., Ngwa, E. M., Aebi, M., and Locher, K. P. (2018) Structure of the yeast oligosaccharyltransferase complex gives insight into eukaryotic *N*-glycosylation. *Science* **359,** 545–550 CrossRef Medline
24. Nasab, F. P., Schulz, B. L., Gamarro, F., Parodi, A. J., and Aebi, M. (2008) All in one: *Leishmania major* STT3 proteins substitute for the whole oligosaccharyltransferase complex in *Saccharomyces cerevisiae*. *Mol. Biol. Cell* **19,** 3758–3768 CrossRef Medline

25. Parodi, A. J. (1993) *N*-Glycosylation in trypanosomatid protozoa. *Glycobiology* **3,** 193–199 CrossRef Medline
26. Fanchiotti, S., Fernández, F., D'Alessio, C., and Parodi, A. J. (1998) The UDP-Glc:glycoprotein glucosyltransferase is essential for *Schizosaccharomyces pombe* viability under conditions of extreme endoplasmic reticulum stress. *J. Cell Biol.* **143,** 625–635 CrossRef Medline
27. Bredeston, L. M., Marino-Buslje, C., Mattera, V. S., Buzzi, L. I., Parodi, A. J., and D'Alessio, C. (2017) The conundrum of UDP-Glc entrance into the yeast ER lumen. *Glycobiology* **27,** 64–79 CrossRef Medline
28. Chavan, M., Suzuki, T., Rekowicz, M., and Lennarz, W. (2003) Genetic, biochemical, and morphological evidence for the involvement of *N*-glycosylation in biosynthesis of the cell wall β1,6-glucan of *Saccharomyces cerevisiae*. *Proc. Natl. Acad. Sci. U.S.A.* **100,** 15381–15386 CrossRef Medline
29. Osumi, M. (2012) Visualization of yeast cells by electron microscopy. *J. Electron Microsc.* **61,** 343–365 CrossRef Medline
30. Lubas, W. A., and Spiro, R. G. (1987) Golgi endo-α-D-mannosidase from rat liver, a novel *N*-linked carbohydrate unit processing enzyme. *J. Biol. Chem.* **262,** 3775–3781 Medline
31. D'Alessio, C., Fernández, F., Trombetta, E. S., and Parodi, A. J. (1999) Genetic evidence for the heterodimeric structure of glucosidase II. The effect of disrupting the subunit-encoding genes on glycoprotein folding. *J. Biol. Chem.* **274,** 25899–25905 CrossRef Medline
32. Kelleher, D. J., and Gilmore, R. (2006) An evolving view of the eukaryotic oligosaccharyltransferase. *Glycobiology* **16,** 47R–62R CrossRef Medline
33. Katoh, T., Takase, J., Tani, Y., Amamoto, R., Aoshima, N., Tiemeyer, M., Yamamoto, K., and Ashida, H. (2013) Deficiency of α-glucosidase I alters glycoprotein glycosylation and lifespan in *Caenorhabditis elegans*. *Glycobiology* **23,** 1142–1151 CrossRef Medline
34. Hardt, B., Völker, C., Mundt, S., Salska-Navarro, M., Hauptmann, M., and Bause, E. (2005) Human endo-α1,2-mannosidase is a Golgi-resident type II membrane protein. *Biochimie* **87,** 169–179 CrossRef Medline
35. Alfa, C., Fantes, P., Hyams, J., McLeod, M., and Wabrik, E. (1993) *Experiments with Fission Yeast: A Laboratory Manual,* 188 pp., Cold Spring Harbor Laboratory Press, Cold Spring Harbor, NY
36. Moreno, S., Klar, A., and Nurse, P. (1991) Molecular genetic analysis of fission yeast *Schizosaccharomyces pombe*. *Methods Enzymol.* **194,** 795–823 CrossRef Medline
37. Sambrook, J., and Russell, D. W. (2001) *Molecular Cloning: A Laboratory Manual*, Cold Spring Harbor Laboratory Press, Cold Spring Harbor, NY
38. Hoffman, C. S., and Winston, F. (1987) A 10-minute DNA preparation from yeast efficiently releases autonomous plasmids for transformation of *Escherichia coli*. *Gene* **57,** 267–272 CrossRef Medline
39. Matsuyama, A., Arai, R., Yashiroda, Y., Shirai, A., Kamata, A., Sekido, S., Kobayashi, Y., Hashimoto, A., Hamamoto, M., Hiraoka, Y., Horinouchi, S., and Yoshida, M. (2006) ORFeome cloning and global analysis of protein localization in the fission yeast *Schizosaccharomyces pombe*. *Nat. Biotechnol.* **24,** 841–847 CrossRef Medline
40. Chino, A., Watanabe, K., and Moriya, H. (2010) Plasmid construction using recombination activity in the fission yeast *Schizosaccharomyces pombe*. *PLoS One* **5,** e9652 CrossRef Medline
41. Hagan, I. M., Carr, A. M., Grallert, A., and Nurse, P. (2016) *Fission Yeast: A Laboratory Manual* (Hagan, I. M., Carr, A. M, Grallert, A., and Nurse, P., eds) 490 pp., Cold Spring Harbor Laboratory Press, Cold Spring Harbor, NY
42. Sato, M., Dhut, S., and Toda, T. (2005) New drug-resistant cassettes for gene disruption and epitope tagging in *Schizosaccharomyces pombe*. *Yeast* **22,** 583–591 CrossRef Medline
43. Soussilane, P., Soussillane, P., D'Alessio, C., Paccalet, T., Fitchette, A. C., Parodi, A. J., Williamson, R., Plasson, C., Faye, L., and Gomord, V. (2009) *N*-Glycan trimming by glucosidase II is essential for *Arabidopsis* development. *Glycoconj. J.* **26,** 597–607 CrossRef Medline
44. D'Alessio, C., Trombetta, E. S., and Parodi, A. J. (2003) Nucleoside diphosphatase and glycosyltransferase activities can localize to different subcellular compartments in *Schizosaccharomyces pombe*. *J. Biol. Chem.* **278,** 22379–22387 CrossRef Medline
45. Stigliano, I. D., Alculumbre, S. G., Labriola, C. A., Parodi, A. J., and D'Alessio, C. (2011) Glucosidase II and *N*-glycan mannose content regulate the half-lives of monoglucosylated species *in vivo*. *Mol. Biol. Cell* **22,** 1810–1823 CrossRef Medline
46. Stigliano, I. D., Caramelo, J. J., Labriola, C. A., Parodi, A. J., and D'Alessio, C. (2009) Glucosidase II β subunit modulates *N*-glycan trimming in fission yeasts and mammals. *Mol. Biol. Cell* **20,** 3974–3984 CrossRef Medline
47. R-Core-Team. (2013) R: A language and environment for statistical computing R Foundation for Statistical Computing, Vienna, Austria
48. Roux, A. E., Quissac, A., Chartrand, P., Ferbeyre, G., and Rokeach, L. A. (2006) Regulation of chronological aging in *Schizosaccharomyces pombe* by the protein kinases Pka1 and Sck2. *Aging Cell* **5,** 345–357 CrossRef Medline
49. Varki, A., Cummings, R. D., Aebi, M., Packer, N. H., Seeberger, P. H., Esko, J. D., Stanley, P., Hart, G., Darvill, A., Kinoshita, T., Prestegard, J. J., Schnaar, R. L., Freeze, H. H., Marth, J. D., Bertozzi, C. R., *et al.* (2015) Symbol nomenclature for graphical representations of glycans. *Glycobiology* **25,** 1323–1324 CrossRef Medline

Abrogation of glucosidase I–mediated glycoprotein deglucosylation results in a sick phenotype in fission yeasts: Model for the human MOGS-CDG disorder

Giovanna L. Gallo, Ayelén Valko, Sofía I. Aramburu, Emiliana Etchegaray, Christof Völker, Armando J. Parodi and Cecilia D'Alessio

J. Biol. Chem. 2018, 293:19957-19973.
doi: 10.1074/jbc.RA118.004844 originally published online November 2, 2018